

---

# DYNAMIC WIRELESS CHARGING BY RESONANT INDUCTIVE POWER TRANSMISSION IN ELECTRIC VEHICLES

---



**By:**

**Fares Ossama Saad**  
**Karim Ashraf El-Kobrossy**  
**Omar Hazem Sabry**  
**Youssef Ahmed Saeed**  
**Zeyad Walaa Gaber**

**Supervised by:**

**Prof. Dr. Ayman Samy**  
**Prof. Dr. Ahmed Abbas**  
**Prof. Dr. Ragi Refaat**

2020

ALEXANDRIA UNIVERSITY  
ALEXANDRIA, EGYPT

## Acknowledgements

Foremost, we would like to thank Allah for enabling us to complete the work on this project. In the light of current events, and what the team has achieved so far from theoretical evaluations to practical implementations, special thanks go to **Prof. Dr. Ayman Samy** who provided us with discrete guidance during practical tests and made sure to facilitate the use of laboratories and college resources within the entire process. Special tribute to **Prof. Dr. Ahmed Abbas** who assured to maintain a proper theoretical evaluation prior to a real-life hardware implementation contributing to the project with a vast knowledge in power electronics. Finally, but not least, appreciation goes to **Prof. Dr. Ragi Refaat** as a result of his proper supervision and dedication to provide a suitable technical environment to his students.

Big thank-you goes to the whole staff of TAs for their continuous assistance and support including **Eng. Mahmoud**, **Eng. Abdelrahman Farghali**, **Eng. Abdallah Shaaweer** and **Eng. Abd El-Rahman Ismail**.

Grateful for the **Academy of Scientific Research & Technology** in Egypt, which offered a generous grant, upon request, sponsoring the entire project and covering any costs to make sure of no obstacles to be met.

It is essential to mention those software packages and CAD programs by the host companies that made it possible to contribute with the entire project:

- **MATLAB**
- **SOLIDWORKS**
- **PROTEUS**
- **ARDUINO**

## Table of Contents

<b>List of Figures.....</b>	<b>6</b>
<b>List of Tables.....</b>	<b>8</b>
<b>1. Chapter 1: Literature Review .....</b>	<b>9</b>
1.1. Electric Vehicles (EVs) history.....	9
1.2. Applications of Wireless Battery Charging .....	10
1.3. Dynamic Power Transfer in Electric Vehicles.....	11
1.3.1. Power Transfer from Overhead lines .....	11
1.3.2. Power Transfer from Conducting Rails Integrated in Road Surface .....	15
1.3.3. Power transfer from conducting rails along the roadside .....	16
1.3.4. Comparative evaluation of concepts for dynamic conductive power transfer.....	18
1.4. Introduction to technologies for dynamic contactless power transfer.....	19
1.5. Advantages of Dynamic Wireless Charging .....	20
<b>2. Chapter 2: System Overview and Components .....</b>	<b>21</b>
2.1. System Overview .....	21
2.2. Overview of Coil Shapes.....	22
<b>3. Chapter 3: High Frequency Inverter Gate Drivers.....</b>	<b>26</b>
3.1. Selection.....	26
3.2. Introduction to TL494 .....	26
3.2.1. Analysis & implementation .....	27
3.2.2. Testing.....	29
3.2.3. Conclusion .....	30
3.3. IR2110 as a MOSFET Driver .....	30
3.3.1. Capabilities: .....	30
3.4. IR2111 as a MOSFET driver .....	30
3.4.1. Capabilities: .....	30
3.4.2. Circuit Schematic:.....	31
3.4.3. Implementation .....	32
3.4.4. Challenges:.....	33
3.4.5. Output: .....	34
3.5. Microcontroller Code .....	35

3.6.	Snubber Circuit .....	36
4.	<b>Chapter 4: Proposed System Details and Design.....</b>	<b>37</b>
4.1.	Electrical Equivalent Circuit .....	37
4.2.	Quality Factor.....	39
4.3.	Bifurcation Phenomenon In an SS-RIPT System .....	40
4.4.	Analytical Electrical Design of Transmitter and Receiver Coils for Bifurcation Free Operation.....	40
4.5.	Analytical Geometrical Design of Transmitter and Receiver Coils.....	43
4.5.1.	Self-Inductance .....	43
4.5.2.	Mutual Inductance .....	44
5.	<b>Chapter 5: Designing a 500 W system.....</b>	<b>45</b>
5.1.	Calculation of Electrical Parameters .....	45
5.1.1.	Secondary Side.....	45
5.1.2.	Primary Side.....	46
5.2.	Calculation of Geometric Parameters .....	48
5.2.1.	Primary Coil.....	49
5.2.2.	Secondary Coil.....	50
5.3.	Coil Manufacturing .....	52
5.4.	Ferrite Addition .....	57
6.	<b>Chapter 6: Simulation Results.....</b>	<b>58</b>
A.	<b>MATLAB PowerSys.....</b>	<b>58</b>
6.1.	AC-DC Rectifier .....	59
6.1.1.	Terminals .....	59
6.1.2.	Parameters.....	59
6.1.3.	Components .....	59
6.2.	H-Bridge.....	60
6.2.1.	Components .....	61
6.2.2.	Terminals .....	61
6.2.3.	Parameters.....	61
6.3.	Primary and Secondary Coils.....	62
6.3.1.	Coils Parameters .....	62
6.4.	AC-DC Rectifier .....	63

6.4.1.	Terminals .....	63
6.4.2.	Parameters.....	63
6.5.	Pure AC voltage Scope .....	64
6.5.1.	Scope Output.....	64
6.5.2.	Parameters:.....	65
6.6.	Rectified AC (DC) Scope.....	65
6.6.1.	Scope Output.....	65
6.7.	Square wave AC (P) Scope (Primary Voltage) .....	66
6.7.1.	Scope Output.....	66
6.8.	Primary Current.....	66
6.9.	Square wave AC (S) Scope (Secondary Voltage) .....	67
6.9.1.	Scope Output.....	67
6.10.	Secondary current .....	67
6.11.	To BMS Scope: .....	68
6.11.1.	Scope Output .....	68
B.	MATLAB SimScape.....	70
C.	Proteus Simulation.....	73
D.	Closed Loop Control.....	74
6.12.	MATLAB Function .....	74
6.13.	System Frequency.....	75
6.14.	System Before Control .....	75
6.15.	System at Steady State.....	76
6.16.	Measuring Phase Shift .....	76
7.	Chapter 7: Experimental Setup and Results.....	77
7.1.	Testing:.....	77
7.1.1.	Static Testing .....	77
8.	Chapter 8: Future Improvements: .....	82
8.1.1.	Dynamic Testing .....	82
8.1.2.	Feedback Control .....	82
8.1.3.	System Synchronization.....	82
8.1.4.	Coil Geometry.....	83
8.1.5.	Litz Wire .....	83
8.1.6.	Ferrite Material .....	83

9.	Chapter 9: Financial Analysis .....	84
9.1.	Prototype .....	84
9.2.	Industrial product .....	85
10.	Chapter 10: Conclusions .....	86
11.	References:.....	93

## List of Figures

Figure 1. 1: Various WPT Techniques .....	10
Figure 1. 2: Power Supply for Road from Transportation Overhead Lines.....	12
Figure 1. 3: Scania Trucks in Operation at the E16 Demonstration Site in Sandviken, Sweden .	13
Figure 1. 4: APS System in Trams & Trucks .....	15
Figure 1. 5: Schematic View of Aistom APS Power Supply System.....	16
Figure 1. 6: Dynamic Charging System Developed by Honda Installed in a Test Track .....	16
Figure 1. 7: Power Take-off System Developed by Honda.....	17
Figure 1. 8: Illustration of Two-Phase Sliding for Power Supply from the Side of the Road.....	17
Figure 1. 9: General Concept of Inductive Power Transfer in EVs.....	19
Figure 2. 1: System Overview .....	21
Figure 2. 2: Various Coil Shapes .....	24
Figure 3. 1: TL494 Functional Block Diagram .....	28
Figure 3. 2: TL494 Output.....	29
Figure 3. 3: Inverter Output Using TL494.....	29
Figure 3. 4: Circuit Schematic .....	31
Figure 3. 5: IR2111 Testing & Implementation.....	31
Figure 3. 6: Challenges .....	33
Figure 3. 7: Signal of Microcontroller .....	34
Figure 3. 8: Signal of Optocoupler .....	34
Figure 3. 9: Signal of IR High Output .....	34
Figure 3. 10: Signal of IR Low Output .....	34
Figure 3. 11: No-load Output Voltage .....	35
Figure 3. 12: Output Before Using Snubber Circuit .....	36
Figure 3. 13: Output After Using Snubber Circuit .....	36
Figure 4. 1: Series-series compensated RIPT circuit .....	37
Figure 4. 2: Simplified Equivalent Model .....	38
Figure 4. 3: Components of SS-RIPT system.....	40
Figure 4. 4: Archimedean Spiral Coil .....	43
Figure 5. 1: Coil Pair P-S1 .....	48
Figure 5. 2: Coil Pair P-S2 .....	48
Figure 5. 3: Coil Pair P-S3 .....	48
Figure 5. 4: Coil Pair P-S4.....	48
Figure 5. 5: Coil Pair P-S5.....	49
Figure 5. 6: Calculated Parameters on EES (Primary Coil).....	50
Figure 5. 7: Calculated Parameters on EES (Secondary Coil).....	51

Figure 5. 8: Primary Coil Base Dimensions .....	53
Figure 5. 9: Secondary Coil Base Dimensions .....	54
Figure 5. 10: Primary Coil .....	55
Figure 5. 11: Secondary Coil .....	56
Figure 5. 12: Primary and Secondary Coils After Adding Ferrite Layer.....	57
Figure 6. 1: Basic System .....	58
Figure 6. 2: AC-DC Rectifier.....	59
Figure 6. 3: H-Bridge.....	60
Figure 6. 4: Primary-Secondary Coils .....	62
Figure 6. 5: Coils Parameters.....	62
Figure 6. 6: AC-DC Rectifier.....	63
Figure 6. 7: Different Scopes in the Simulation .....	64
Figure 6. 8: Pure AC Voltage Scope Output.....	64
Figure 6. 9: Pure AC Voltage Scope Parameters.....	65
Figure 6. 10: Rectified AC (DC) Scope Output.....	65
Figure 6. 11: Square wave AC (P) Scope Output .....	66
Figure 6. 12: Primary Current.....	66
Figure 6. 13: Square wave AC (S) Output .....	67
Figure 6. 14: Secondary Current .....	67
Figure 6. 15: To BMS Scope Output .....	68
Figure 6. 16: Full Circuit Using SimScape .....	69
Figure 6. 17: Full Implementation of Both MATLAB Simulation and Practical Sensors .....	70
Figure 6. 18: Relay Circuit.....	71
Figure 6. 19: Proteus Simulation .....	72
Figure 6. 20: Primary Voltage and Current .....	72
Figure 6. 21: Feedback Control System.....	73
Figure 6. 22: Frequency Variation .....	75
Figure 6. 23: Initial Voltage & Current .....	75
Figure 6. 24: Voltage & Current at Zero Phase Shift .....	76
Figure 6. 25: Phase Shift Variation.....	76
Figure 7. 1: Testing Mechanism .....	77
Figure 7. 2: Primary Current.....	80
Figure 7. 3: Primary Voltage .....	80

## List of Tables

Table 1. 1: Comparison Between Different Types of Dynamic Conduction.....	18
Table 2. 1: Different Coil Shapes .....	25
Table 5. 1: Electrical Parameters .....	47
Table 5. 2: Coils' Final Parameters .....	51
Table 7. 1: Testing at 40 Input Voltage .....	78
Table 7. 2: Testing at 60 Input Voltage .....	79
Table 7. 3: Testing at 80 Input Voltage .....	79
Table 7. 4: Testing at 80 Input Voltage .....	80
Table 9. 1: Components' Costs .....	84

## 1. Chapter 1: Literature Review

The main goal of this research was to formulate clear design guidelines for fabrication and control of an efficient series-series resonant inductive power transfer (SS-RIPT) system for electric vehicle battery charging application. In meeting this objective, several critical shortages about the field of RIPT based EV chargers specific to stationary charging have been solved.

### 1.1. Electric Vehicles (EVs) history

In 1900, electric cars were about one-third of all vehicles on the road of U.S.A, and then almost disappeared from the landscape as gasoline-engine models took over. However, the main reason for this disappearance was their limited driving range and their relatively higher cost compared to gasoline-powered engines at that time. Decades later, technological advances, concerns about the environment, and increasing oil prices pushed towards their gradual revival -which is not so gradual anymore- as electricity can be produced by using non-polluting and continuously renewable energy sources. By 2040, more than half of all new cars worldwide will be powered only by batteries, according to Bloomberg New Energy Finance anticipations. The continuous increase in interest in electric vehicles has led to an increase in interest in developing new charging techniques. Traditionally, EVs most often used charging method is simple plug-in charging and sometimes be known as conductive charging or plug-in charging in which an ordinary copper connected cable forms the power link. This method is widely used and accepted in the market, and it is available for most EVs by Tesla, Chevrolet, and Mercedes-Benz. However, there are some drawbacks to plug-in charging, such as safety concerns caused by exposed plugs and damaged cables, and the long period for a full charge. To avoid these drawbacks, wireless charging methods have been widely studied over the past few years.

The concept of wireless transfer of power, however, has been around since the late 1890s. Nikola Tesla was able to light electric bulbs without using wires at his Colorado Springs Lab using electro-dynamic induction, known as resonant inductive coupling.

Wireless power transfer (WPT) has been studied using various techniques, such as Acoustic, Light, Microwave, Laser, Capacitive, and Inductive Wireless Power Transfer. The name wireless power transmission means the transfer of electrical power from a source to an electrical device without the help of a physical medium (wires). Basically, it involves two coils: a transmitter coil connected to a primary electronic circuit and a receiver coil connected to a secondary electronic circuit. The basics of WPT depends on the inductive energy transmission from a transmitter to a receiver through a variation in the magnetic field. To get this DC current, that is supplied by a power source, it is converted into high-frequency AC current by the aid of the specially designed electronics built in the primary circuit. What distinguishes the different types of WPT is the “medium of power transfer” between both the receiver and transmitter coils. It has been found that the Inductive Power Transfer (IPT) has the potential to transfer medium to high power needed in the application of EVs battery charging. This method can also be referred to as resonant inductive power transfer (RIPT), inductively coupled power transfer (ICPT), and

contactless power transfer (CPT). **Figure (1.1)** shows a list of the various WPT technologies as well as the form of power transfer:

Technology	Energy Transfer	Enabling the Power Transfer
Inductive coupling	Magnetic fields	Coils of wire
Resonant inductive coupling	Magnetic fields	Resonant circuits
Capacitive coupling	Electric fields	Conductive coupling plates
Magnetodynamic coupling	Magnetic fields	Rotating permanent magnets
Microwave radiation	Microwaves	Phased arrays/dishes
Optical radiation	Light/infrared/ultraviolet	Lasers/photocells

**Figure 1. 1:** Various WPT Techniques

## 1.2. Applications of Wireless Battery Charging

The applications of wireless battery charging are increasing dramatically these days to include all types of appliances and accessories that used to work using ordinary cables. The different types of applications can be classified as follow:

- **Smart Phones, Portable Media Players, Digital Cameras, Tablets and Wearables:** Consumers are asking for easy-to-use solutions, increased freedom of positioning, and shorter charging times. These applications typically require 2 W to 15 W of power. Multi-standard interoperability is preferred. Wireless charging can coexist with NFC (Near Field Communication) and Bluetooth, allowing for very creative solutions. For example, paired phones can charge each other up when placed back-to-back, after they negotiate the appropriate host and client.
- **Accessories:** Headsets, wireless speakers, mice, keyboards, and many other applications can benefit from wireless power transmission. Plugging charging cables into the tiny connectors of ever-shrinking devices is an impediment to robust design. For example, Bluetooth headsets need to be sweat proof to survive in a gym environment. Only wireless charging can enable that possibility.

- **Public Access Charging Terminal:** Deployment of charging pads (transmitters) in the public domain requires systems to be safe and secure. But smart charging systems can go well beyond stand-alone charging solutions. They can enable quick network-connectivity and create billable charging stations if desired. Many coffee shops, airport kiosks and hotels support these scenarios. Furniture manufacturers also design-in discreet wireless power transmitters into their end and side tables.
- **Computer Systems:** Laptops, notebooks, ultra-books and tablet PCs are all candidates for wireless charging as either hosts or clients. The possibilities are endless.
- **In-Cabin Automotive Applications:** A wireless charger is ideal for charging mobile phones and key fobs by placing them either on the dash or the center console of the car, without inconvenient wires going to the cigarette lighter socket. Moreover, since Bluetooth and Wi-fi require authentication to connect phones to car electronics, combining NFC with wireless charging can enable the user to not only charge the phone, but to automatically connect it to the car's Wi-fi and Bluetooth networks without going through any specific setup process.
- **Electric Vehicles:** Smart charging stations for EVs (electric vehicles) are also coming up but require much higher powers. Standards are under development.
- **Miscellaneous:** Wireless chargers are finding its way into anything with a battery inside it. This includes game and TV remotes, cordless power tools, cordless vacuum cleaners, soap dispensers, hearing aids and even cardiac pacemakers. Wireless chargers are also capable of charging super capacitors (super caps), or any device that is traditionally powered by a low-voltage power cable.

### 1.3. Dynamic Power Transfer in Electric Vehicles

The wireless charging topic is a vast topic with a lot of challenges ahead, However, this book will concentrate on the most important challenging topic which is the dynamic power transfer in electric vehicles. Nowadays, there are different forms and structures proposed for charging electric vehicles efficiently and only few are implemented and are still in their testing phase.

#### 1.3.1. Power Transfer from Overhead lines

A concept for electric power supply from overhead lines as shown in **figure (1.2)** has been developed and promoted by several companies. The technology is partly developed on basis of equipment and standards for light rail systems and trolley-busses, with adaptations mainly related to the power take-off system and the mechanical interface to the vehicle. **Figure (1.3)** shows Scania Trucks in operation at the E16 demonstration site in Sandviken, Sweden.

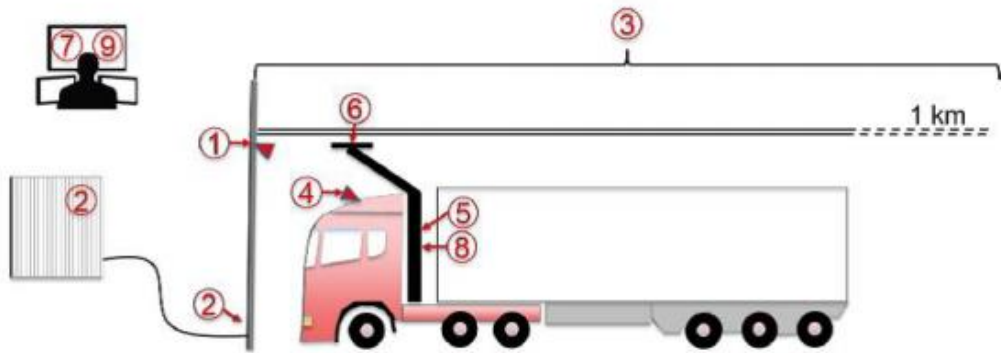


**Figure 1. 2:** Power Supply for Road from Transportation Overhead Lines

#### A) General description of concept

- 1) The physical infrastructure for continuous power supply along the road, is similar to the power supply systems of overhead lines for trams or railway systems, although two conductors with independent contacts to the vehicle are necessary.
- 2) Connection to a sub-station for power supply from the distribution network (typically 11 or 22 kV in Scandinavia). The substation includes equipment for fault detection and disconnection of line sections in case of emergencies or failure.
- 3) Sections of about 1 km of continuous overhead lines, supplied separately from the substation.
- 4) The presence of overhead lines above the vehicle must be detected before the on-board power take-off equipment can be activated. The detection is in this case based on a laser scanner, which is also used to illustrate the position of the lines with respect to the pantograph of the power take-off system as a visual feedback to the driver of the vehicle.
- 5) The mechanical position control of the power take-off arms, which includes continuous position tracking of the overhead lines during driving.
- 6) The pick-up system, based on a pantograph with two arms, where each arm provides two contact points for its corresponding conductor.
- 7) Power measurements from the sub-station with online feedback to a control center.

- 8) On-board power conversion system for control of power flow and interfacing of the power supply with the on-board electrical drive system and energy storage unit. The onboard equipment can also include metering devices for monitoring and billing of the electricity consumption of each vehicle.
- 9) Operation and control center for monitoring the operation of the system.



**Figure 1. 3:** Scania Trucks in Operation at the E16 Demonstration Site in Sandviken, Sweden

B) The status of this technology can be summarized as:

- 1) The technology is based on conventional and well-proven concepts, where the actively position-controlled power take-off unit is the main new addition compared to systems for railways and trolley-busses.
- 2) A demonstration site in practical road traffic is operation in Sweden since 2016, and 6 months of demonstration on a public road in California has been completed during 2017. Three demonstration projects on public roads in Germany are planned for operation in 2018–2019.
- 3) Currently considered to be at TRL level 7, but no technical constraints are expected for reaching TRL level 8 or 9.
- 4) It is expected that such systems can be quickly implemented if there is will for investment.
- 5) The sub-stations of such systems could easily be designed for bidirectional power flow, as has been implemented in the test track in Germany [14]. However, the demonstration facility in Sweden is not designed for power flow from the overhead lines back to the utility grid. In general, it is not expected that there will be any need for bidirectional power flow in flat areas or roads with relatively high and regular traffic.
- 6) The main technical disadvantage in terms of operation and scalability is that the concept can only be used for large vehicles like trucks and busses. However, only the technical functionality is considered in this document, and no attempts are made to quantify the potential economic advantages and disadvantages of providing infrastructure for all types of vehicles in a regular traffic pattern.
- 7) Since installed overhead lines will not influence regular traffic or the road surface, they can potentially coexist with other solutions for dynamic power transfer to moving vehicles based on conductive or inductive technology integrated in the road cross-section at or below the surface. Thus, technology for conductive or inductive power transfer to smaller vehicles could for instance be installed on selected parts of a road with overhead lines for powering long distance heavy freight transportation.
- 8) The main disadvantage for public acceptance is expected to be the visual impact of overhead lines, although this will likely be of less concern for large scale highways with high traffic density. However, this concept is not considered suitable for city environment due to concerns regarding public acceptance of the visual impact.

### 1.3.2. Power Transfer from Conducting Rails Integrated in Road Surface

Several concepts for power transfer to moving vehicles from conducting rails integrated in the ground surface have been proposed during the last years. Such systems have already been implemented for city trams, to avoid the visual impact of poles and overhead lines needed for catenary systems.

One of the concepts under development is based on adaptation of technology for trams, while other systems are developed specifically for road vehicles. **Figure (1.4) & Figure (1.5)** shows how the system operates.

The motivations for developing concepts allowing for dynamic power transfer from conductive infrastructure integrated in the road surface has been mainly to overcome the limitations in terms of applicability for electric road systems based on overhead lines. Thus, the two main advantages that should be obtained with such systems are:

- Possibility for vehicles in a wide range of sizes to utilize the infrastructure
- Avoiding the installation and corresponding visual impact of overhead lines.

The second point has also been a driving motivation for developing city tram systems supplied from the road surface.

a) Tram with APS in operation [23]



b) Testing of truck with adapted APS system [21]



**Figure 1. 4: APS System in Trams & Trucks**

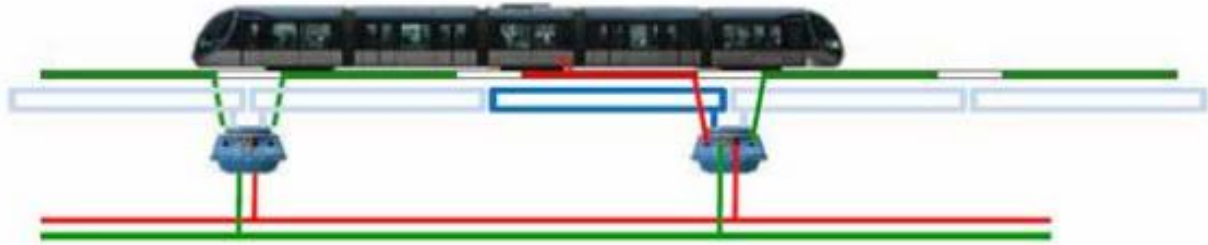


**Figure 1. 5:** Schematic View of Aistom APS Power Supply System

### 1.3.3. Power transfer from conducting rails along the roadside

The concept under development by Honda is based on power take-off with a mechanically controlled arm that can be extended from the vehicle to the power supply rail integrated in the safety fence along the road. **Figure (1.6) and Figure (1.7)** shows the dynamic charging system developed by Honda installed in a test track.



**Figure 1. 6:** Dynamic Charging System  
Developed by Honda Installed in a Test Track

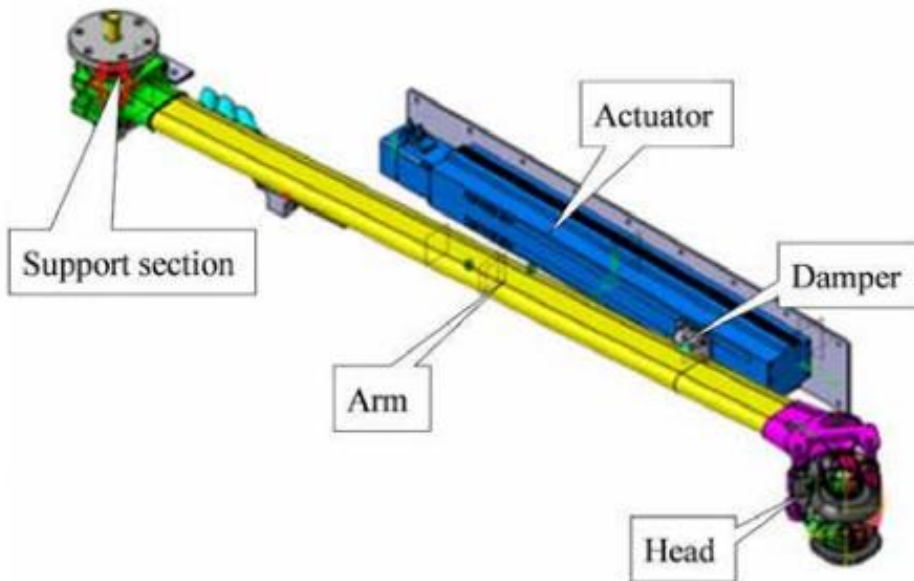


**Figure 1. 7:** Power Take-off System Developed by Honda

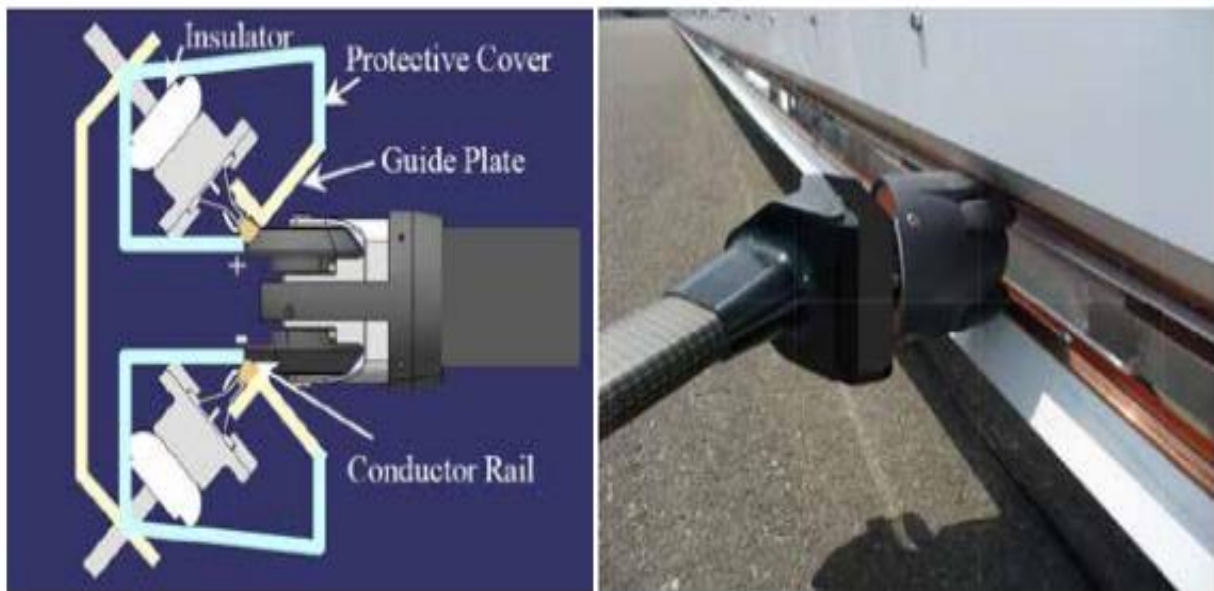


**Figure 1. 8:** Illustration of Two-Phase Sliding for Power Supply from the Side of the Road

### 1.3.4. Comparative evaluation of concepts for dynamic conductive power transfer

**Table (1.1)** compares different concepts for dynamic conductive power transfer including their advantages and disadvantages.

	<b>Advantages</b>	<b>Disadvantages</b>	<b>Technology Status</b>
<b>Overhead lines Siemens</b>	<ul style="list-style-type: none"> <li>• Simple system</li> <li>• Based on mature technology</li> <li>• No impact on road surface</li> <li>• Proven operation under wide range of weather and climate conditions</li> </ul>	<ul style="list-style-type: none"> <li>• Only suitable for large vehicles</li> <li>• Visual impact</li> <li>• Active positioning of power- take-off</li> </ul>	<ul style="list-style-type: none"> <li>• Ready for utilization</li> <li>• TRL 7 by 2018 and no technical obstacles expected to reach 8/9</li> <li>• Low risk for pilot projects</li> </ul>
<b>Rail solution Alstom EPS</b>	<ul style="list-style-type: none"> <li>• Limited visual impact</li> <li>• Experience with similar technology for trams</li> <li>• Can be used for smaller vehicles</li> </ul>	<ul style="list-style-type: none"> <li>• Energized conductor in road surface</li> <li>• Short rail sections and high number of switches</li> <li>• Complicated system for energization according to vehicle position</li> <li>• Need for active positioning of power take-off unit</li> <li>• Concerns regarding reliability and maintenance requirements</li> <li>• Low friction on conductors</li> </ul>	<ul style="list-style-type: none"> <li>• Based on available components</li> <li>• Currently around TRL 4</li> <li>• Adaptations needed for large-scale utilization</li> <li>• Uncertain reliability in Norwegian conditions</li> <li>• Limited design possibilities for avoiding increased wear of conductors and road surface during winter conditions</li> </ul>
<b>Rail solution Elways</b>	<ul style="list-style-type: none"> <li>• Limited visual impact</li> <li>• Can be used for smaller vehicles</li> <li>• No energized conductors at road surface</li> </ul>	<ul style="list-style-type: none"> <li>• Need active positioning for connecting to road-integrated rail</li> <li>• High expected wear on vehicle-side conductor</li> </ul>	<ul style="list-style-type: none"> <li>• Based on simple technology</li> <li>• Currently around TRL 6</li> <li>• Uncertain reliability in Norwegian conditions, especially in case of salty and humid environment</li> </ul>
<b>Rail solution Elonroad</b>	<ul style="list-style-type: none"> <li>• -Limited visual impact</li> <li>• Only single sliding contact in the road surface with alternating polarity for each section</li> <li>• Limited need for integration in the cross-section of the road</li> </ul>	<ul style="list-style-type: none"> <li>• Energized conductor in road surface</li> <li>• Short rail sections and high number of switches</li> <li>• Concerns regarding reliability and maintenance requirements</li> </ul>	<ul style="list-style-type: none"> <li>• Currently TRL 4</li> <li>• Further trials expected</li> <li>• Uncertain reliability in Norwegian conditions</li> </ul>
<b>Rail solution Honda</b>	<ul style="list-style-type: none"> <li>• Similar advantages as surface- integrated solutions in terms of applicability and efficiency</li> <li>• No installation in the road surface</li> <li>• Potentially simpler position control of power take-off system</li> </ul>	<ul style="list-style-type: none"> <li>• Safety in case long sections are energized</li> <li>• Safety issues related to arm for power-take-off</li> </ul>	<ul style="list-style-type: none"> <li>• -Demonstrated on dedicated test-track</li> <li>• Limited information available in English</li> <li>• Main concerns are related to safety and practical applicability</li> </ul>

**Table 1. 1:** Comparison Between Different Types of Dynamic Conduction

## 1.4. Introduction to technologies for dynamic contactless power transfer

The basic principle of the power transfer is that current in a coil integrated in/below the road surface generates a magnetic field. The magnetic coupling (i.e. mutual inductance) between the transmitting coil in the road and the receiving coil integrated in the vehicle determines to which extent this field influences the receiving coil.

The rate of change of the magnetic field generated by the transmitting coil generates a voltage in the receiving coil, which drives the current into the on-board power conversion system and by that transfers electric power to the vehicle. Due to the coupling between the coils, the current in the receiving coil is also influencing the magnetic field and generates a counter-induced voltage in the transmitting coil. Thus, the system operates with alternating currents (AC), and the frequency of operation has significant impact on the design and power transfer capability of such a system.

In general, the physical principles determining the operation of inductive power transfer systems are the same as for a conventional transformer, with the main difference that the coupling between the transmitting and receiving coils is much lower than in a conventional transformer for power system applications due to the significant airgap between the two coils. **Figure (1.8)** shows the general concept of inductive power transfer in electric vehicles.

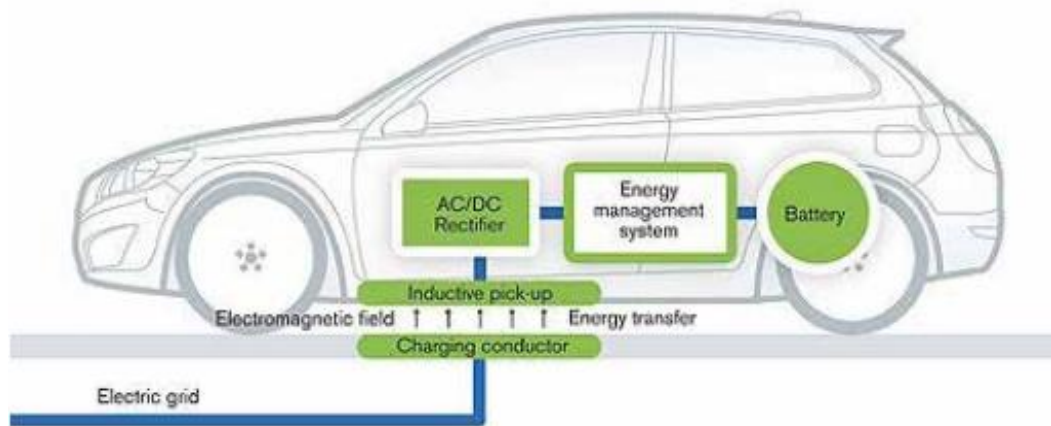


**Figure 1. 9:** General Concept of Inductive Power Transfer in EVs

## 1.5. Advantages of Dynamic Wireless Charging

- I. Range Extension:** Dynamic wireless charging has what is called “opportunity charging” i.e. the vehicle can be charged at the same time it is traveling from one place to another without the need for lengthy stops during a single trip. These opportunity charging are possible since wireless charging does not require complete stop and human intervention, therefore charging can be carried out automatically. This, in turn, leads to significant improvements in range compared to that available from a conventional plug-in charge.
- II. Battery Volume Reduction:** Another advantage of “opportunity charging” which allow charging more frequently, EVs can cut the same distance with a smaller battery pack. This, in turn, will lower the price of EVs and make them more efficient due to their reduced weight. Frequent charging extends the battery life as well by reducing the depth of discharge in the battery.
- III. Safety and Convenience:** Wireless charging provides complete isolation between load and source which by turn, eliminate any risks accompanied with plug-in charging method such as the risk of electric shock -especially in a wet environment-, the wear of contactors caused by excessive use and thermal cycling and, most importantly, discomfort in handling a plug-in charger in a harsh climate that usually may have snow and where the charging points may become frozen onto the vehicle itself.
- IV. Weatherproof:** In a wireless power transfer system, the power transfer takes place by an electromagnetic link, therefore the charging is not much affected by the contamination of snow, rain, or dust. Moreover, a transmitter is embedded underground, therefore, it is safe from extreme weather conditions and requires less frequent maintenance or replacement than a plug-in charger would require.

Due to the aforementioned advantages, in the following chapters, a full study will be introduced to learn more about inductive power transmission and the design procedures of a full battery charging system.

## 2. Chapter 2: System Overview and Components

In this chapter a brief overview will be proposed including the different system's components and a detailed study for different types of coils used in the transmitter and receiver pads.

### 2.1. System Overview

**Figure (2.1)** shows the power flow for a resonant inductive power transfer (RIPT) system starting from the grid 220V/50Hz supply until the car battery charger. Firstly, the AC voltage is rectified using full bridge rectifier to obtain a constant DC voltage. Secondly, a high-frequency square wave is generated using a high-frequency inverter to supply the primary coil and its compensation capacitor.

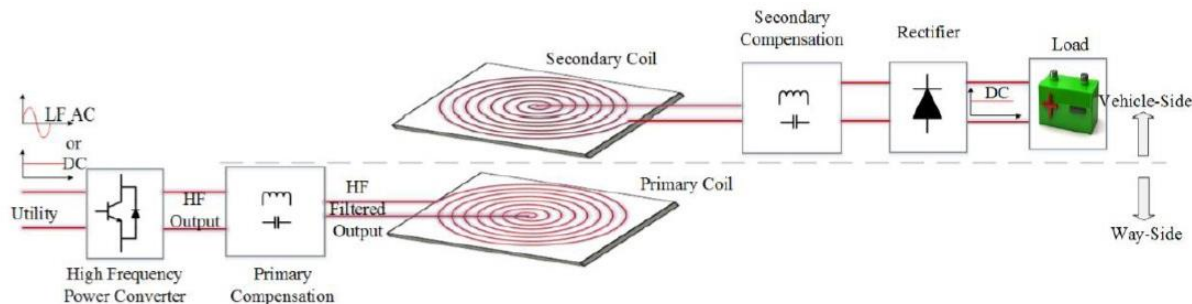


**Figure 2. 1:** System Overview

This high-frequency voltage generates energy in the form of a high-frequency current through a compensation circuit and primary coil. A primary compensation circuit (capacitor) is added to make the primary input voltage and the current in phase to minimize the VA-rating and thus the size of the high-frequency power inverter. Moreover, primary compensation also acts as a bandpass filter when resonating with the coil's inductance at the designed frequency blocking undesirable frequency components generated from the power electronic inverter feeding the primary. Therefore, an almost sinusoidal current flows in the primary coil and this enables soft-switching operation of the inverter feeding the primary coil.

Energy is then transferred to the car side through the magnetically coupled secondary coil with the primary one by the flux generated in the air gap between them. There is a secondary compensation circuit (capacitor) as well to improve the power transfer capability of the system. Lastly, the received voltage is rectified again to obtain constant DC voltage required to supply the loads and charge the batteries through the car's BMS (battery management system).

Compensating circuits, which are capacitors, are made to resonate with coil inductance, thus forming a resonant inductive link. There are four types of resonant inductive links depending on the way of connection of the compensating capacitor with the primary and secondary coils which are: series-series (SS), series-parallel (SP), parallel-series (PS) and parallel-parallel (PP). Primary

parallel compensation such as (PP) and (PS) resonant inductive links allows using a higher value of primary current as only a small part of the current flows through the semiconductor. However, (PP) and (PS) have several drawbacks.

Firstly, they require an additional series inductor to regulate the inverter current flowing into the primary resonant tank.

This series inductor increases the inverter size and, therefore, the total cost of the whole system. Secondly, due to the circulating current in the primary resonant tank, the partial load efficiency of the parallel compensated primary system is lower. Thirdly, in (PP) and (PS) resonant inductive links, the value of the primary compensation capacitor is not constant but varies as the mutual coupling and load vary. Therefore, (PP) and (PS) resonant inductive links will need further complicated control strategies to maintain unity power factor operation in the primary power supply regardless of the load and mutual coupling variation. Primary series compensation helps to cancel the significant voltage drop of the primary coil; therefore, the required voltage rating of the power supply is reduced. In (SS) and (SP) resonant inductive links, no extra inductor is needed unlike (PS) and (PP). Moreover, primary compensation is independent of load. However, in an (SP) resonant inductive link, primary compensation depends upon the mutual coupling between the two coils also and therefore, needs consideration in the application of dynamic charging. The (SP) resonant inductive link requires a higher value of capacitance for stronger magnetic coupling and its peak efficiency is less than (SS) resonant inductive link. Therefore, a (SS) resonant inductive link is theoretically the best regarding efficiency, number of components, the complexity of control, and cost, hence it was chosen.

## 2.2. Overview of Coil Shapes

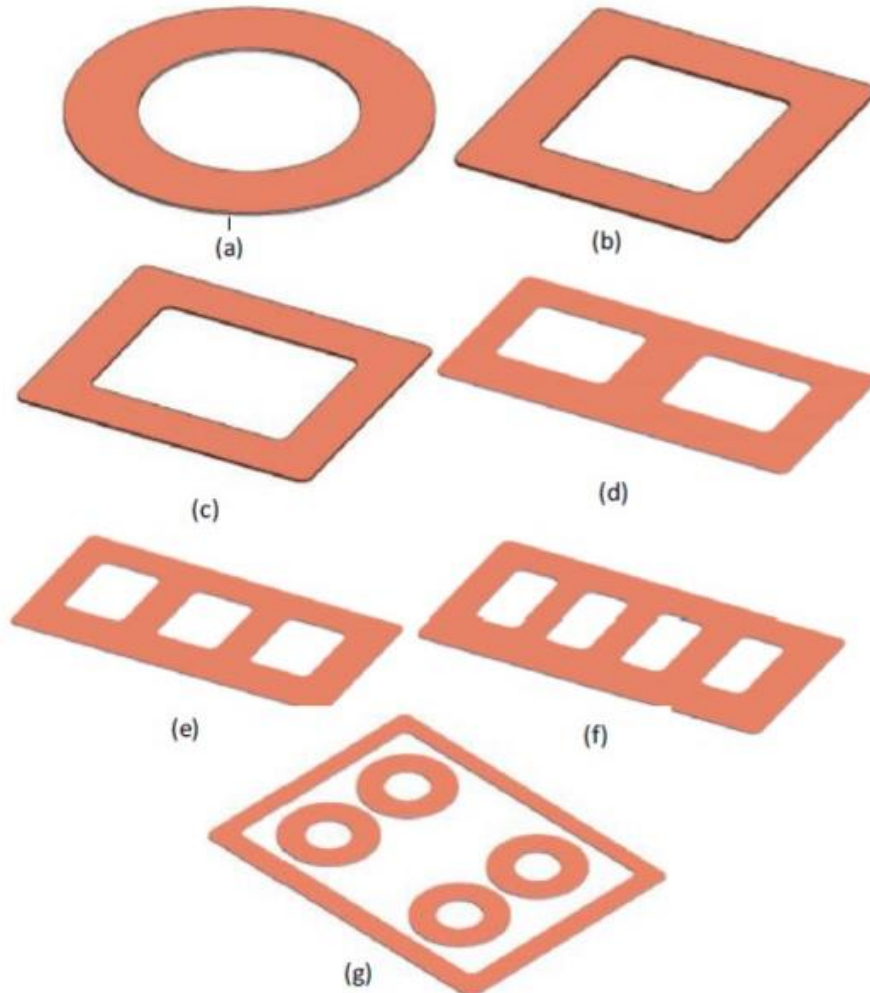
In wireless charging systems for EVs, the concept of air-core wireless transformer is utilized to transfer several amounts of power ranges from few watts to kilowatts from the transmitter to the receiver side. As shown in **Figure (2.2)**, different types of planar coil shapes such as circular, rectangular, and hybrid arrangements can be used while designing the wireless transformer to improve the charging performance and to solve problems related to misalignment between the transmitter and receiver coil pads. Wireless charging coils are mainly categorized into two areas: polarized pads (PPs) and non-polarized pads (NPPs).

Polarized pads are combinations of multiple coils and shapes to generate perpendicular (vertical) and parallel (horizontal) components of the magnetic flux. PPs are made by arranging multiple shape coils in certain arrangements. Such shapes are compatible with single-phase applications as well as for three-phase applications. Solenoidal coil, Double D (DD), Double D Quadrature (DDQ), Bipolar (BP), and Quad D Quadrature (QDQ) are all examples of the (PPs). Solenoidal coils which can generate a sharp arching polarized magnetic field on both sides of the pad are made by winding the coils around a flat ferrite plate. This can be done by connecting two wound coils magnetically in series and electrically in parallel. These polarized fluxes are higher than the NPP's fluxes. Double D (DD) polarized pads are made by combining two square or rectangular

coils that generate flux in only one direction (opposite to the ferrite plate) with negligible leakage fluxes at the edge. From its significant advantages is that it covers both horizontal (X & Y) and vertical directions. In addition, this design can produce an excellent coupling coefficient and quality factor for the coil at no load. Due to the higher tolerance of the horizontal misalignment, this pad is suitable for primary coupling in both stationary and dynamic applications. The Double D Quadrature (DDQ) coil is the advanced version of the DD pad with the generation of twice the flux height generated by the basic circular pad.

In addition to the features of DD pads, it also provides a considerable improvement on the issues related to lateral misalignment with the manufacturing flexibility of Q coil. The DDQ coupler is suitable for the application of both the single or three-phase power source, either primary or secondary. It is considered an excellent choice to be used as a secondary coil as it is able to collect both sine and cosine magnetic flux vectors. Bipolar (BP) charging pads are created from various similar size coils. BP is much economical in terms of used copper with around 25 to 30% less copper for the construction when compared to the DDQ pad. Though, it drops the coupling coefficient by around 13% with 30° angular misalignment between the primary and secondary pads. Quad D Quadrature (QDQ) pads have been introduced to improve the overall performance, including flux height to reach the receiver and misalignment. Such shapes use two or more circular and square coils to design wireless transformers. Quad D Quadrature pad offers a considerably high coupling coefficient and can transfer enough amount of power with 50% misalignment displacement.

On the other hand, non-polarized pads (NPPs) are created from a single-coil shape to produce perpendicular (vertical) components of magnetic flux only. NPPs are the conventionally shaped coils, such as circular, rectangular, square, and hexagonal. The circular coil is well-known and widely used in transformers because their eddy currents are minimum as there are no sharp edges. By adjusting the inner diameter, the distribution of the magnetic flux can be controlled. For smaller inner diameters, the magnetic field section would be spike-shaped, which helps in improving the coupling coefficient. Increasing the inner diameter can expand the magnetic flux distribution areas which can assist in the problems concerning misalignment. Rectangular and square shaped coils are appropriate when they require certain arrangement in an array as their sides are perfectly aligned. However, they increase coil inductance because the sharp corners generate eddy current and increase the coil impedance and hot areas. This is why it is unsuitable for high-power applications. Rectangular shape coils have greater horizontal misalignment tolerance when compared to circular and square coils.



Coil shapes (a) Circular (b) Square (c) Rectangular (d) Double D (e) Bi-polar  
(f) Double-D quadrature (g) Quad-D quadrature.

**Figure 2. 2:** Various Coil Shapes

However, hexagonal coils present the maximum power transfer efficiency at zero misalignment between the transmitter and receiver coils, but with a significant loss in the power when it reaches the edge of the coil. Oval shaped coils can provide more misalignment tolerance, but they are not appropriate with high power applications as they have poor performance with the horizontal misalignment.

Circular pads (CPs) are non-polarized pads and are easier to operate and have the same tolerance to misalignment in all directions. They are non-directional, i.e. a vehicle can approach them from any direction. The circular geometry is still the most widely used for its simplicity, despite having a lower coupling coefficient than other coil geometries with the same size, air gaps, and misalignment. Therefore, a circular pad has been adopted for designing the wireless charger for EVs.

**Table (2.1)** summarize the difference between different coil shapes

	<b>CRP</b>	<b>CP</b>	<b>HP</b>	<b>DDP</b>	<b>DDQP</b>	<b>BPP</b>
<b>Transferrable power</b>	Medium	Medium	Low	High	High	High
<b>Pad design size</b>	Medium	Medium	Large	Small	Small	Small
<b>Pad weight</b>	Low	Low	High	Low	Medium	Medium
<b>System material cost</b>	Low	Low	High	Medium	High	Medium
<b>Transmission distance</b>	Low	Low	Medium	Medium	High	High
<b>Charging zone</b>	Small	Small	Large	Medium	Large	Large

**Table 2. 1:** Different Coil Shapes

### 3. Chapter 3: High Frequency Inverter Gate Drivers

Dynamic wireless charging systems, being proposed, have brought up solutions to multiple complications of occupying an EV -as mentioned previously-, yet introduced several challenges where each requires high technology applications to deal with.

This project had some special requirements and speaking for the inverter requirements the complexity can be summarized in designing a high power and high-frequency gate driver up to 120 kHz given the hardware complications and resonance effect challenges. High frequency and power applications turned out to be tricky and never was easy.

A frequency of 40 kHz is selected to work within this paper so as to match available resources and provide a level of simplicity

#### 3.1. Selection

In order to achieve such a DC/HF AC converter, a proper design of a control circuit, acting as a pulse generator driving a full bridge, was to be constructed. Integrated circuits of different kinds were proposed, each of unique characteristics where the most outstanding were the IR2111, IR2110 & TL494.

In this paper, the selection of an IR2111 was proven to come in handy, although a working design of a TL494 has been implemented and tested successfully. TL494 circuit will be presented explaining its drawbacks, followed by a brief description of an IR2110, then a detailed discussion of an IR2111 circuit to be next.

#### 3.2. Introduction to TL494

The TL494 is originally a pulse width modulation IC, as old as it was invented yet it is still - along with some other similar IC's - one of the most powerful and widely used IC's in many applications.

TL494 is a pulse-width modulation control chip invented in 1975 - by Texas instruments - spurred the development of switching power supplies, leading to a power control IC industry that today is measured in billions of dollars.

### 3.2.1. Analysis & implementation

Although many PWM IC's such as the TL494 were invented a few decades back yet firing the four MOSFET's gates in the right order while effectively controlling many aspects such as duty cycle, dead time, etc... Especially at high frequencies was not that easy.

It would have taken us much more time to design this complex high-frequency gate driver if it wasn't for those PWM IC's, and while searching through many other options such as SG1524, MC3420, and many others the special TL494 turned out to be the most suitable - also available - for this application.

This unique IC incorporates all the functions required in the construction of a pulse-width-modulation (PWM) control circuit on a single chip. Designed primarily for power-supply control, this device offers the flexibility to tailor the power-supply control circuitry to a specific application.

The TL494 contains two error amplifiers, an on-chip adjustable oscillator, a dead-time control (DTC) comparator, a pulse-steering control flip-flop, a 5V / 5% precision regulator, and output-control circuits. The error amplifiers exhibit a common-mode voltage range from  $-0.3$  V to  $V_{CC} - 2$  V. The dead-time control

The comparator has a fixed offset that provides approximately 5% dead time. The on-chip oscillator can be bypassed by terminating RT to the reference output and providing a sawtooth input to CT, or it can drive the common circuits in synchronous multiple-rail power supplies.

The uncommitted output transistors provide either common-emitter or emitter-follower output capability. The TL494 provides for push-pull or single-ended output operation, which can be selected through the output-control function. The architecture of this device prohibits the possibility of either output being pulsed twice during push-pull operation. **Figure (3.1)** illustrates the functional block diagram of the TL494.

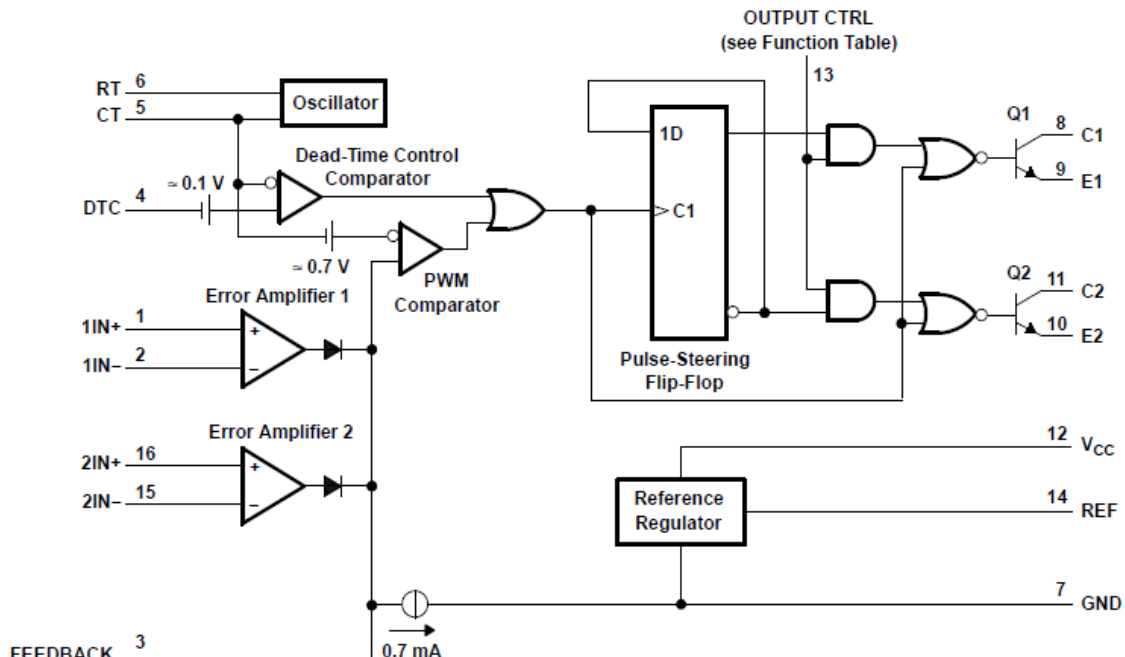


**Figure 3. 1: TL494 Functional Block Diagram**

The TL494 stands for its easy implementation, it is a really smart solution that ends and terminates other highly complex solutions. As shown in the functional block diagram above, the IC offers exactly what is needed for operation in a 16-pin dual in-line package and offers reliable and easy control of each option.

The IC oscillator circuit has a clearly improved performance than alike IC's, also offers an easy way to control the frequency using a resistor and capacitor connected at pins 5 and 6 offering precise control of the frequency over a wide range (1 – 300) kHz which is quite amazing. Also, pin 4 allows for control of dead time when in push-pull operation which was not needed in our case as the IC already offers a suitable built-in dead time.

The two error amplifiers also weren't used in our case, they can be used for current control in other applications along with some other circuitry and feedback from the output, and you can also neglect them and control the output using the feedback pin connected internally to the outputs of the error amplifiers.

### 3.2.2. Testing

The circuit was connected after spending much time studying and researching for the exact desired output signal and it was then tested to give a precise and nearly perfect output as shown in **figure (3.2)** ready to fire the inverter's MOSFET gates. **Figure (3.3)** shows the inverter's output after being fired by the TL494.

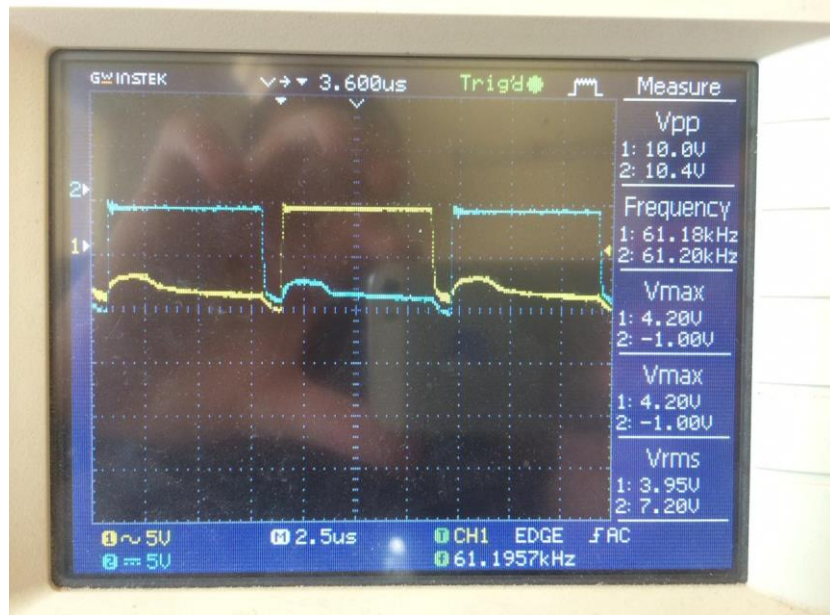


Figure 3.2: TL494 Output

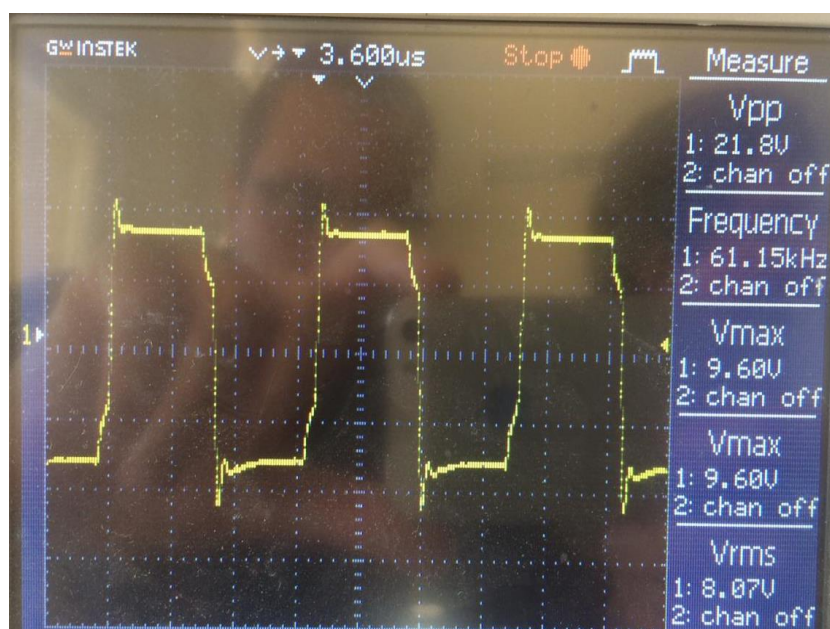


Figure 3.3: Inverter Output Using TL494

### 3.2.3. Conclusion

Unfortunately, despite the many advantages of this powerful IC (high frequency, high power for gate pulses, smooth and stable operation, adjustable dead-time control, etc....) it was then decided to use an entirely different way for firing pulses using a gate driver which is fed from a dedicated microcontroller (AVR) as it is available by few lines of code to achieve closed-loop frequency control which is necessary to maintain resonance by continuously measuring the power factor for the output.

## 3.3. IR2110 as a MOSFET Driver

### 3.3.1. Capabilities:

- 1) Independent high and low output channels.
- 2) The high side having a maximum voltage of 500 volts.
- 3) Being able to supply a 10 to 20-volt gate drive.
- 4) A frequency of up to 5 MHz can be achieved.
- 5) Bootstrap capacitor needed to introduce a certain level of complexity.
- 6) Ton/toff of 120 ns & 94 ns respectively.
- 7) **Schmitt triggered inputs.**
- 8) **Matched propagation delay for both channels.**
- 9) **Deadtime, bandwidth, and duty-cycle are to be set manually using a microcontroller introducing a level of complexity but still extremely useful in high-frequency applications.** (Such an advantage was not considered in this paper due to its undesirable complications.

## 3.4. IR2111 as a MOSFET driver

### 3.4.1. Capabilities:

Pretty much the same as an IR2110 but with a unique characteristic of an internally set deadtime of 650 ns introducing some sort of permeability and allowing a simple frequency control, accordingly the IR2111 was selected as a gate driver.

### 3.4.2. Circuit Schematic:

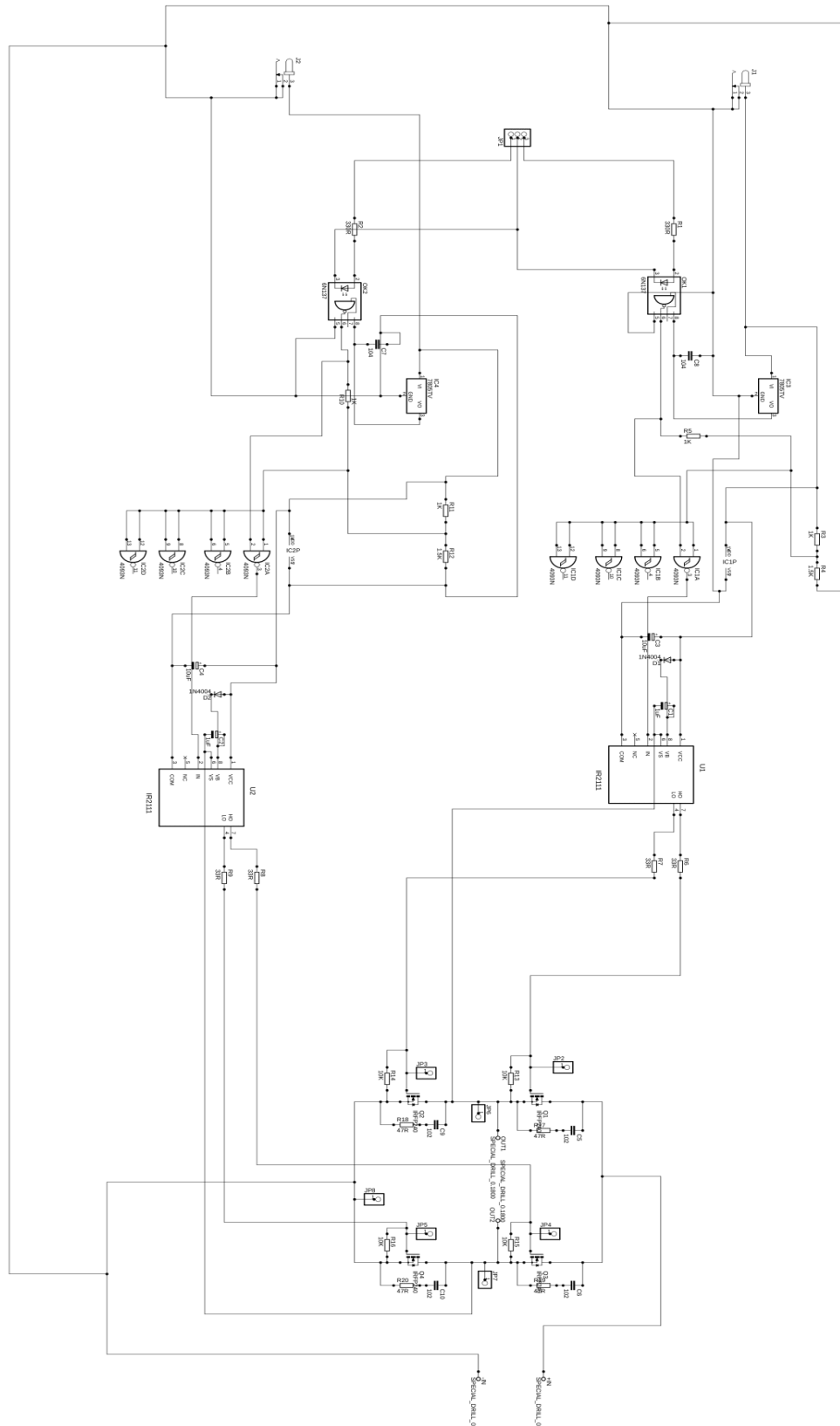


**Figure 3. 4: Circuit Schematic**

### 3.4.3. Implementation

- 1) 2 inverted square wave signals are sent from a microcontroller of a type “ATTINY” at a frequency of 40 kHz.
- 2) Signals are converted to 2 separate optocouplers of type “6N136” serving as an isolator.
- 3) Schmitt trigger is added between the optocoupler’s output and the input of an IR2111.
- 4) Bootstrap capacitance added according to calculations.
- 5) Having 2 separate circuits of common ground, each providing 2 gate signals sent to 2 different power MOSFETs.
- 6) Gate resistance values are critical and chosen upon calculations.

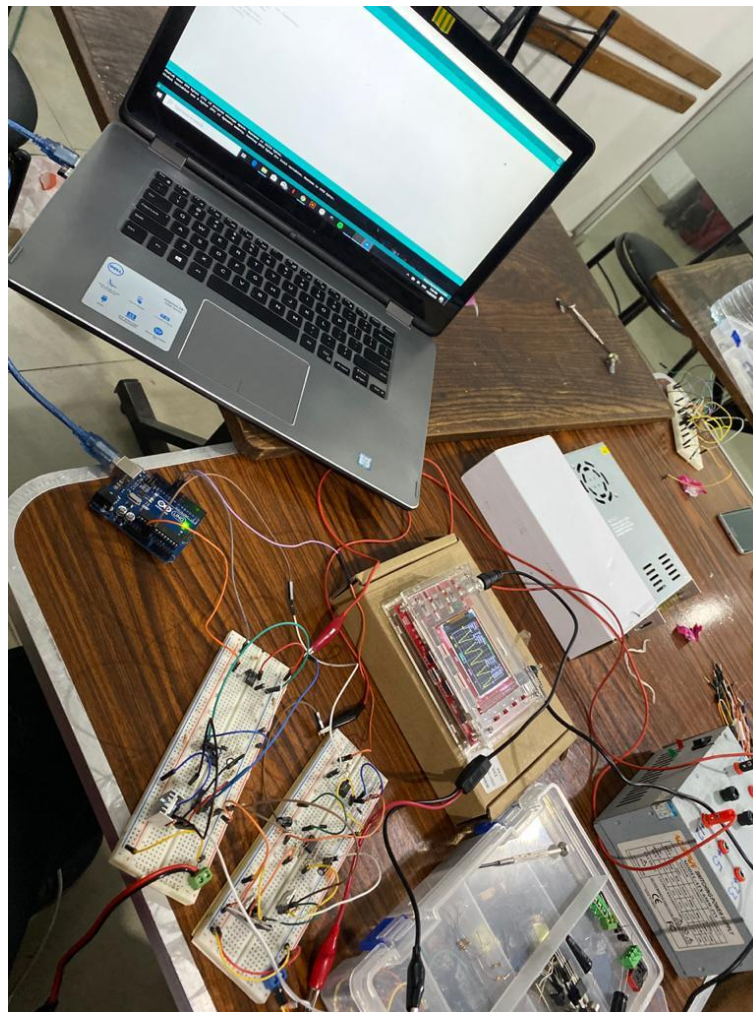


**Figure 3. 5:** IR2111 Testing & Implementation

### 3.4.4. Challenges:

- 1) Measurements: wave characteristics were first tested using a DIY DSO oscilloscope showing, to some extent, accepted measurements of frequency, duty cycle and waveforms, until more accurate results of waveforms were to be measured using a proper oscilloscope neglecting noise and taking into consideration mixed signals.
- 2) Hardware Complications: using uncertified ICs was introducing a series of unexpected events, one was the relatively large rise and fall times of an optocoupler 6N136 leading to a 0-volt output at the beginning of each half cycle which consequently lead to a 25% of power loss as shown in figure.

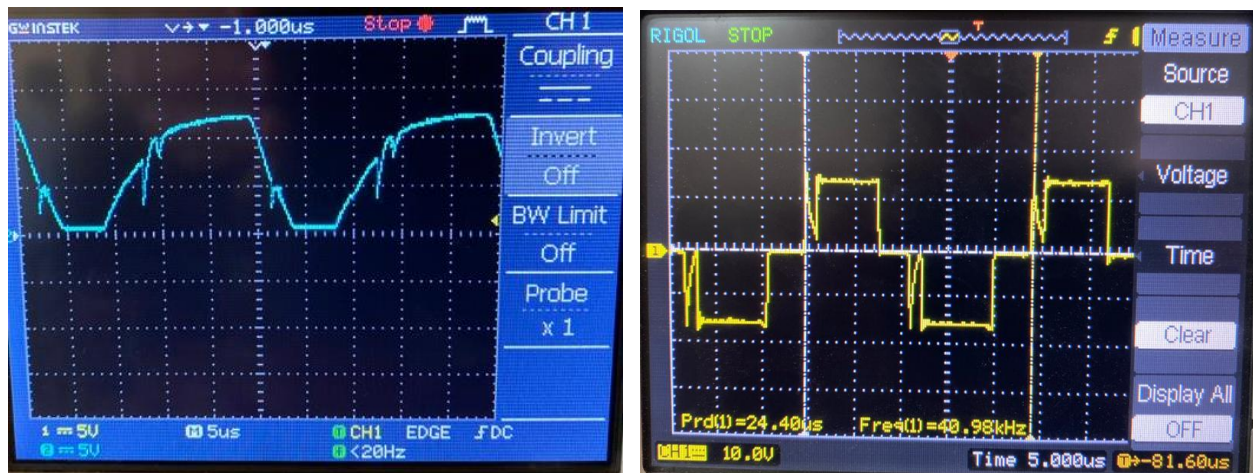
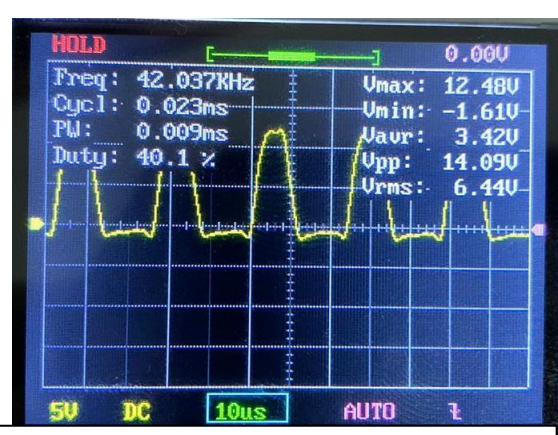
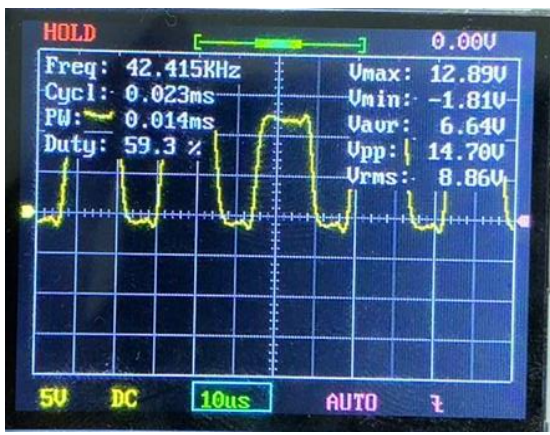
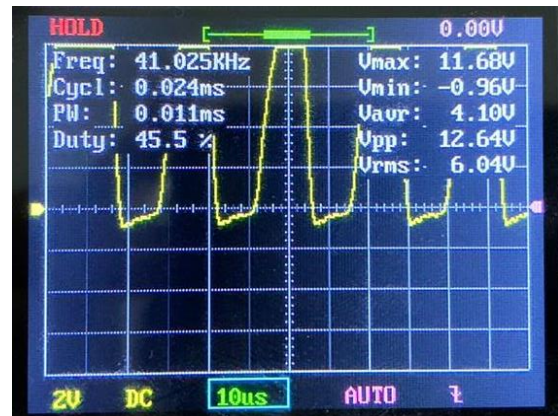
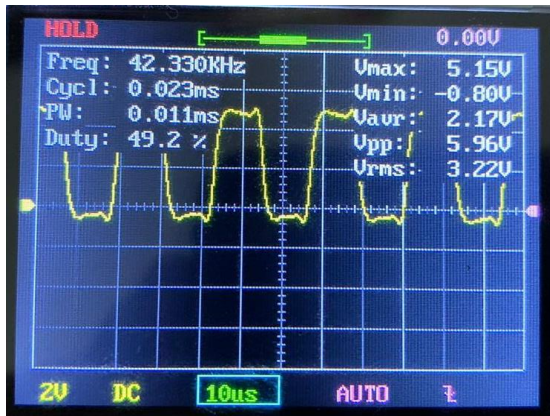


**Figure 3. 6: Challenges**

Solution for previous problem was connecting a schmitt trigger in series with the optocoupler output as mentioned before ensuring a square wave input, due to hysteresis effect, to the IR2111.

### 3.4.5. Output:

- 1) Signals of microcontroller, optocoupler, IR's high-output and low-output in the first testing phases are shown respectively:



- 2) No-load output voltage of an almost perfect square wave was achieved at a frequency of 40KHz.

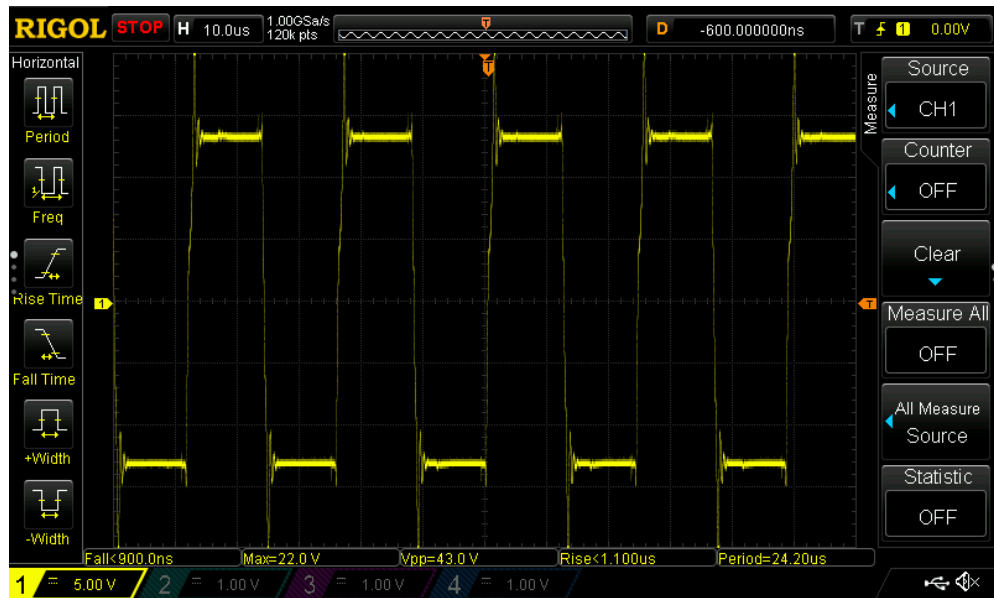


**Figure 3. 11:** No-load Output Voltage

### 3.5. Microcontroller Code

```
#include <avr/io.h>

int main(void)
{
    /*this code uses ATMEGA32 microcontroller to generate two
    square waves on pins OC0 & OC2 -(PB3 & PD7) using timer
    module "CTC MODE" with a prescaler of Fosc/16 and waves
    are inverted, OC2 is inverted signal of OC0*/
    DDRD |= (1<<7);
    DDRB |= (1<<3);
    TCCR0 = 0b10111010;
    TCCR2 = 0b10101010;
    OCR0 =24;
    OCR2 =24;
    TCCR0 = 0b10011010;
    TCCR2 = 0b10011010;
    while (1)
    {
    }
}
```

### 3.6.Snubber Circuit

The first trial of testing the entire system witnessed an unexpected voltage output of the primary coil initiating each half cycle with high frequency oscillations -as shown in **figure (3.12)**- around the expected steady maximum and minimum voltages.

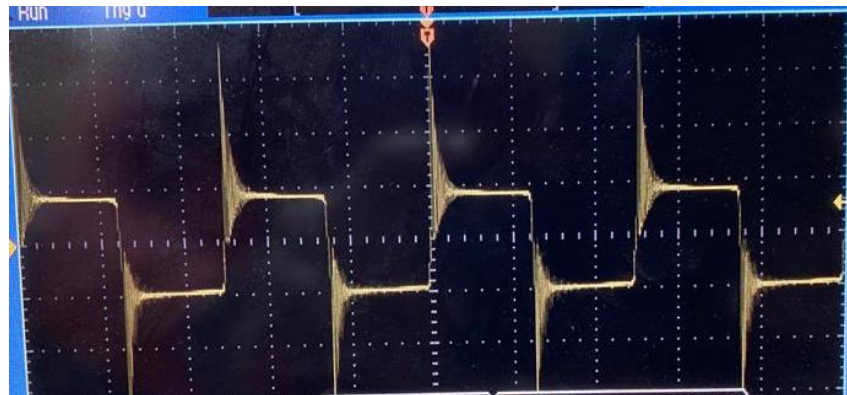


**Figure 3. 12:** Output Before Using Snubber Circuit

It was due to the high frequency switching MOSFETs, and consequently, it was solved by adding a 4 snubber circuits, each containing of a resistor and a capacitor in series, and then connected in parallel to each MOSFET. The new output is shown in **figure (3.13)**.

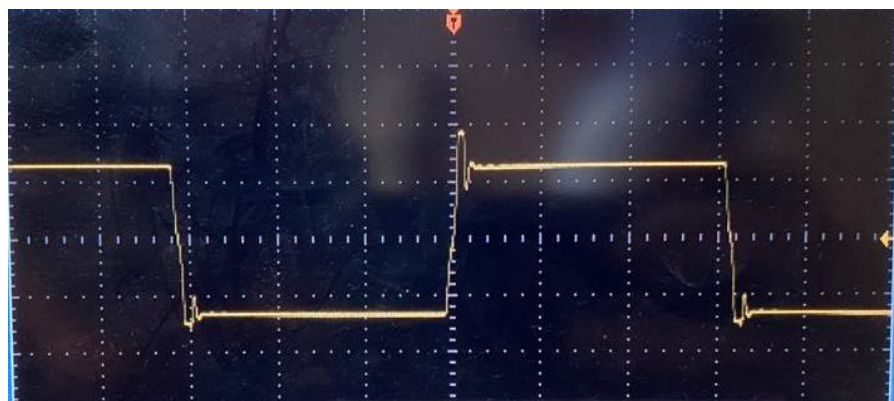


**Figure 3. 13:** Output After Using Snubber Circuit

## 4. Chapter 4: Proposed System Details and Design

In the following chapter a design procedure will be presented which calculates the parameters of coils, such as self and mutual inductance, for the desired power transfer in such a way that the bifurcation phenomenon can be avoided at the design level. After calculating the electrical and circuit parameters of coils, geometric parameters, such as size, numbers of turns, turns spacing will be analytically computed. The importance of the quality factor which is an important feature for an RIPT system will be explained as well. In addition to this, the best unsymmetrical coil shape with the best magnetic characteristics and the least sensitive to misalignment will be chosen according to the most recent researches. Following the design guidelines and design consideration for an Archimedean spiral, a 500 W wireless charging pad will be designed for the SS-RIPT system.

### 4.1. Electrical Equivalent Circuit

The equivalent circuit of a series-series compensated resonant inductive power transfer (SS-RIPT) system is presented in **Figure (4.1)**. The primary side of the SS-RIPT link is fed from the voltage-sourced full-bridge inverter which converts the DC voltage obtained from the rectifier  $V_{dc}$  into high-frequency AC voltage  $V_{AB}$ . On the secondary side, a full-wave rectifier with a capacitive filter  $C_f$  converts the high-frequency AC voltage into DC voltage  $V_o$  and DC current  $I_o$  required by the load ( $R_o$ ). (SS) topology acts as a current source when the primary is supplied from the voltage-source at the ideal resonant condition. Therefore, a simple capacitive filter is sufficient.

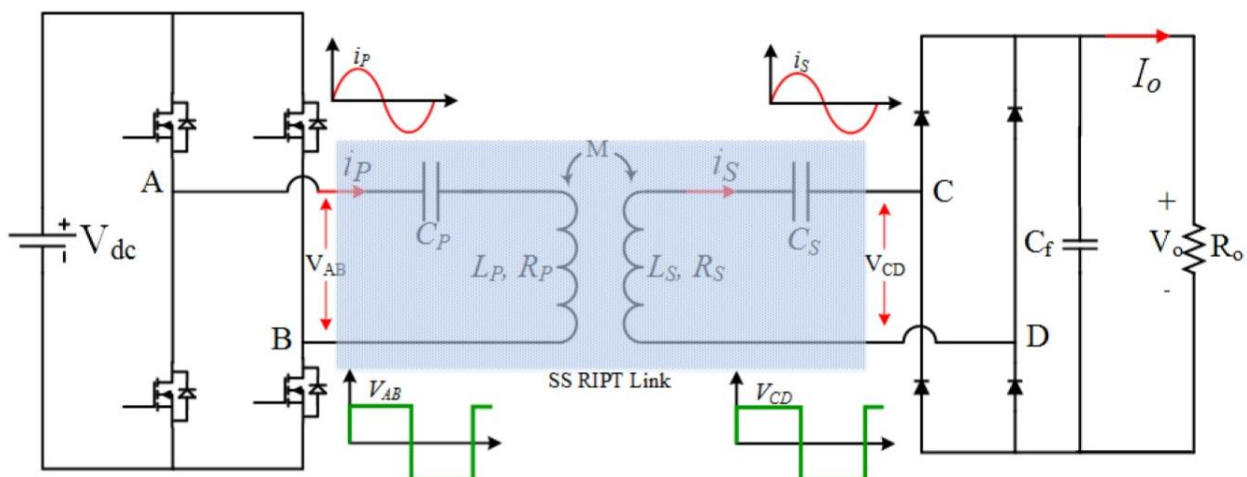


**Figure 4. 1:** Series-series compensated RIPT circuit

A full-bridge inverter produces a square wave voltage  $V_{AB}$ , which contains an infinite number of harmonics. However, the SS-RIPT link acts as a bandpass filter that blocks undesirable frequency components generated from the power electronic converter feeding the primary. Therefore, the current flowing through the RIPT link is almost sinusoidal.

**Figure (4.2)** shows the simplified equivalent model of the circuit illustrated in **Figure (4.1)**.

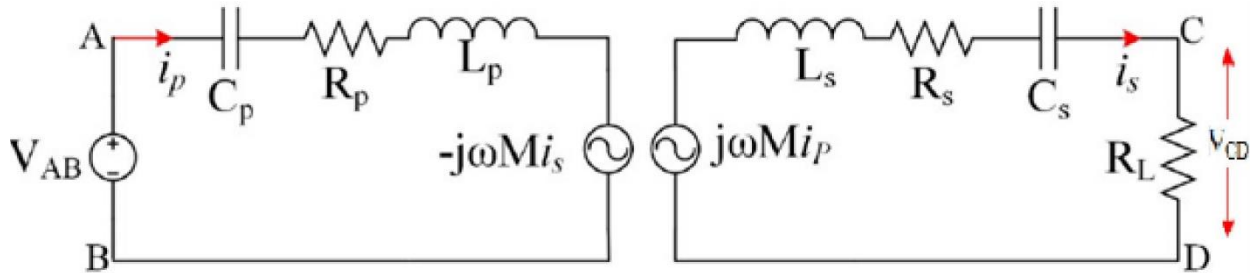


**Figure 4. 2:** Simplified Equivalent Model

In **figure(4.2)**,  $C_p$ ,  $C_s$ ,  $R_p$ ,  $R_s$ ,  $L_p$ ,  $L_s$ ,  $M$  and  $\omega$  represents the primary compensation capacitor, secondary compensation capacitor, primary coil resistance, secondary coil resistance, primary coil self-inductance, secondary coil self-inductance, the mutual inductance between the coils and the operating frequency, respectively. The primary coil is compensated (made to resonate with self-inductance of the primary coil) to minimize the VA rating of the supply hence improving the power factor (unity) whereas the secondary winding is compensated to enhance the power transfer capability of the system. The value of the primary and secondary capacitor for an SS-RIPT system can be calculated by:

$$C = \frac{1}{\omega^2 \times L}$$

$\omega$  represents the resonant frequency of the circuit. Since the primary capacitor is made to resonate with the self-inductance of the primary coil, it acts as the sharply tuned bandpass filter, and therefore, the primary current  $I_p$  is almost sinusoidal. Due to the transformer action, the secondary current  $I_s$  is also nearly sinusoidal.

At this stage, it is important to explain two important concepts of the RIPT system which are: the quality factor and the bifurcation phenomenon. These two concepts are essential to be considered while designing the coils of an RIPT system for enhanced performance.

## 4.2. Quality Factor

It is worth noting that the quality factor can be given to an individual component or a complete circuit. When given to an individual component, it is used to indicate the purity of the reactive element and is known as the intrinsic quality factor  $Q_i$ . For example, in Figure (equivalent circuit), the intrinsic quality factor of the secondary coil is given by:

$$Q_{i-Ls} = \frac{\omega \cdot L_s}{R_s}$$

It is obvious that the intrinsic quality factor is inversely proportional to the self-resistance of the coil. It is used to indicate ‘the goodness of a reactive component’. A low self-resistance of the coil, or in other words a high intrinsic quality factor of a coil is advantageous for low power dissipation in the form of copper loss. Therefore, a high value of the quality factor is necessary for any circuit to keep the losses minimum.

The quality factor can also be defined as how many times the voltage across the reactive element is more than the voltage of the supply and can be defined as the ratio between the voltage across the inductor or the capacitor -in a series resonant circuit- to the voltage across the load resistance in the circuit, which is given by:

$$Q = \frac{\text{Voltage across inductor or capacitor}}{\text{Voltage across resistor}}$$

This indicates that a high-quality factor can lead to a dangerously high voltage across the insulation and may result in electrical breakdown if not handled carefully. For example, in Figure (equivalent circuit), if the voltage across the load resistance is 400 V and the voltage drop across the self-resistance of the coil is neglected, then for  $Q_s$  of value 10, the voltage across the inductor and capacitor terminal would be about 4 kV. Therefore, a component of higher ratings would be required. In addition, the cable joining these components together will also require extra insulation.

From the above discussion, it can be concluded that the selection of the quality factor requires a compromise between component ratings and losses in the system. Usually, in practical applications, a value of 2 to 10 is chosen for  $Q$ .

### 4.3. Bifurcation Phenomenon In an SS-RIPT System

In this section, the bifurcation phenomenon will be discussed and how to avoid its occurrence. The RIPT system is a double-tuned circuit i.e. two capacitors are added to form two resonant tanks with primary and secondary coil self-inductances. The primary capacitor is chosen that the high-frequency inverter which acts as the primary power source has a minimum possible VA rating, i.e., the primary voltage and current are in phase. In such a circuit, it is very common to have more than one zero phase angle (ZPA) frequency. This phenomenon is known as the bifurcation phenomenon or pole splitting where more than one ZPA frequency exists. Identifying the real ZPA frequency is necessary for enhancing system efficiency and power transfer capability.

It was found in order to avoid the bifurcation phenomenon the value of coupling coefficient (K) which is given by:

$$K = \frac{M}{\sqrt{L_p \cdot L_s}}$$

Must be less than a critical value given by:

$$K_{cr} = \frac{1}{Q_s} \sqrt{1 - \frac{1}{4Q_s^2}}$$

### 4.4. Analytical Electrical Design of Transmitter and Receiver Coils for Bifurcation Free Operation

**Figure (4.3)** shows the block diagram and components of an SS-RIPT based wireless charger. The main goal is to calculate the electrical parameters of the SS-RIPT link (shown in the red dotted box) for a given load (battery pack).

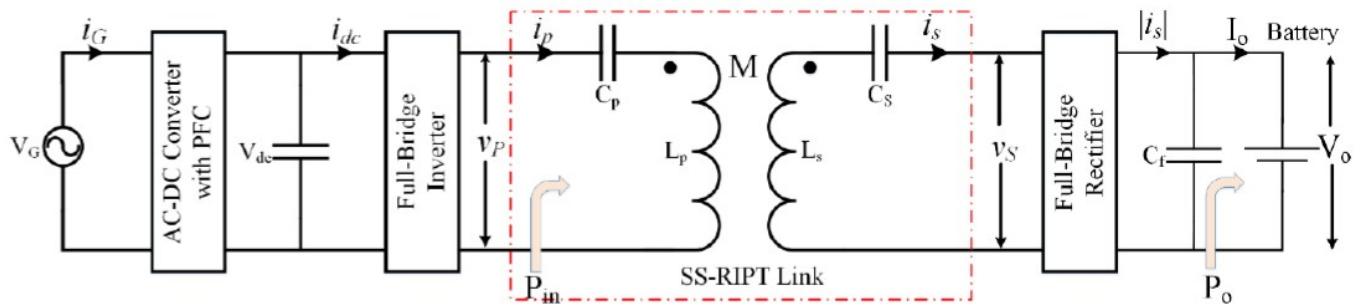


**Figure 4. 3:** Components of SS-RIPT system

Some assumptions were made to simplify the calculation of the electrical parameter:

1. The efficiency of the SS-RIPT system is assumed to be 100%. This assumption is reasonable since the value of coil resistance is unknown before the design of the system, and therefore it is assumed to be negligible.
2. Only the fundamental component (first harmonic) of the input voltage  $V_{AB}$  and output voltage  $V_{CD}$  of the SS-RIPT link is considered and higher order harmonics are neglected. In other words, the quality factors of the primary and the secondary circuit are assumed to be high to obtain sinusoidally varying primary and secondary currents.
3. All the switching components are considered ideal with zero commutation time (i.e. they turn on and off instantaneously) and zero on-resistance (i.e., when conducting they do not present any voltage drop or losses). In other words, all converters are assumed to have an efficiency of 100%.
4. Ideal resonance in the primary and the secondary sides is assumed.

Let the desired output power be  $P_o$ . Since the load is a battery pack, therefore the desired charging voltage is known, as defined by the manufacturer of the battery pack. Let  $V_o$  be the output voltage or the nominal charging voltage. The battery can then be represented by a resistance  $R_o$  as:

$$R_o = \frac{V_o^2}{P_o}$$

The AC equivalent of a DC resistance with a diode rectifier and a capacitive output filter can be given by:

$$R_L = \frac{8}{\pi^2} \cdot R_o$$

This is the value of resistance as seen by the secondary side of the SS-RIPT link.

The secondary side voltage  $V_s$  is a square wave, due to the capacitive output filter. Therefore, the RMS value of the fundamental component of  $V_s$  can be given by:

$$V_{s-RMS} = 2\sqrt{2} \cdot \frac{V_o}{\pi}$$

And the value of RMS secondary current  $I_s$  can be given by:

$$I_{s-RMS} = \frac{V_{s-RMS}}{R_L}$$

From the first assumption, since  $P_o$  is assumed equal to  $P_{in}$  therefore, the RMS value of the primary current  $I_p$  can be given by:

$$I_{p-RMS} = \frac{P_o}{V_{P-RMS}}$$

Where the primary RMS voltage equal to the grid voltage after being rectified then inverted (square wave).

Once the value of the primary and the secondary current are calculated, the value of the mutual inductance ( $M$ ) for the desired amount of output power can be derived by applying KVL equation on the secondary side of the SS-RIPT link where:

$$M \cdot I_p \cdot \omega = R_L \cdot I_s$$

Therefore:

$$M = \frac{R_L \cdot I_s}{I_p \cdot \omega}$$

The secondary inductance can be calculated from the secondary quality factor  $Q_s$ . As discussed before, the value of  $Q_s$  should be selected between 2 and 10 as a higher value can make the system difficult to tune, and a lower value will lead to harmonics in the waveform of current and the voltage. The following equation gives the value of the required secondary inductance:

$$L_s = \frac{Q_s \cdot R_L}{\omega}$$

The value of the coupling-coefficient  $k$  can be obtained using the equation of the critical coupling as mentioned before. To avoid bifurcation, the value of  $k$  should be selected to be less than  $k_c$ , which is:

$$K_{cr} = \frac{1}{Q_s} \sqrt{1 - \frac{1}{4Q_s^2}}$$

The previous equation will decide the minimum air gap between the primary and the secondary coils. It also tells that the maximum value of the coupling-coefficient, exceeding it will lead the system into the bifurcating mode and therefore having a coupling-coefficient as high as possible is not a good design practice and should be better avoided. This is an important difference between a loosely coupled system such as the SS-RIPT system and a closely coupled ( $k=1$ )

system such as power transformers in which it is desirable to have a coupling coefficient as high as possible. Once the value of  $k$  is decided, the primary inductance can be calculated using by:

$$L_p = \frac{M^2}{L_s \cdot K^2}$$

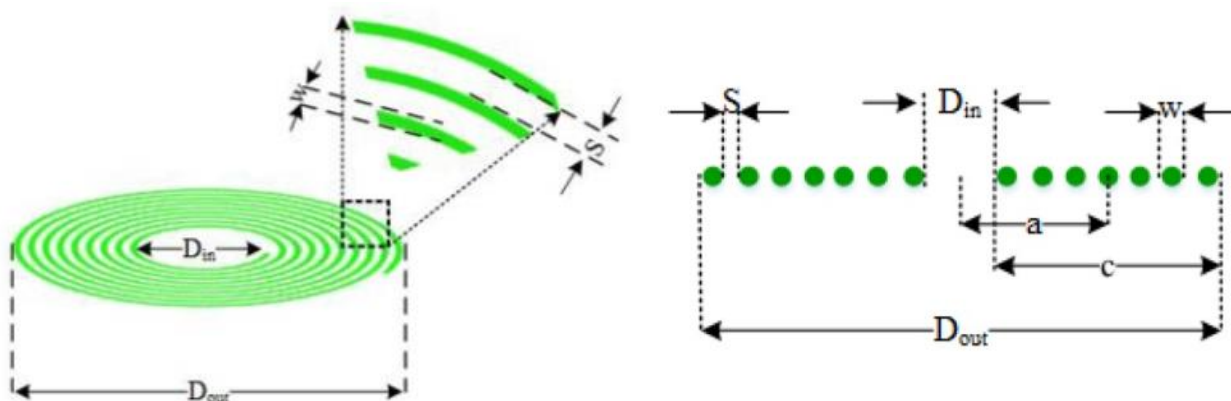
After calculating the parameters for the SS-RIPT link. The next stage is physically building the coils from the calculated values which will be discussed in the following section.

#### 4.5. Analytical Geometrical Design of Transmitter and Receiver Coils

In this section, guideline equations will be presented to achieve the calculated parameters in the previous section as the self-inductance and the mutual inductance of the coil by adjusting the geometric parameters such as inner diameter, outer diameter, inter-turn spacing and distance between the coils.

##### 4.5.1. Self-Inductance

Accurate physical modeling of the Archimedean Spiral Coil (inductor) is important since it is difficult to modify the spiral once built. Wheeler presented several formulas for planar spiral inductors, which were intended for the discrete inductors, they are primarily based on empirical measurements, and are accurate to a few percent. For our project, an amended form of the original Wheeler formula for an Archimedean spiral coil has been used to calculate the geometric parameters of the spiral coil from the estimated value of self-inductance. **Figure (4.4)** shows the representation of an Archimedean spiral.



3D View of Archimedean Coil

Cross-section View of Archimedean Coil

**Figure 4.4:** Archimedean Spiral Coil

From **Figure (4.4)** it is obvious that  $D_o$  is the outer diameter;  $D_{in}$  is inner the diameter;  $S$  is the spacing between turns, and  $w$  is the diameter of the wire used for making the coil. The following equation gives the original Wheeler expression for calculating the inductance of spiral coils in  $\mu\text{H}$  when all the dimensions are in inches and “N” is the number of turns:

$$L = \frac{a^2 N^2}{8a + 11c}$$

From **figure (4.4)** “a” and “c” can be calculated by:

$$c = \frac{D_o - D_{in}}{2}$$

$$a = \frac{D_o - c}{2} = \frac{D_o + D_{in}}{4}$$

Putting “a” and “c” in the inductance equation and converting the units, a modified and more usable version of the Wheeler formula can be derived as shown:

$$L = \frac{N^2 (D_o + D_{in})^2}{8(15D_o - 7D_{in})2.54}$$

The previous equation gives the inductance of spiral coils in  $\mu\text{H}$  when all the dimensions are in cm. And the following equation related the outer diameter ( $D_o$ ), inner diameter ( $D_{in}$ ), turns spacing (s), wire diameter (w) and the number of turns (N):

$$D_o = D_{in} + 2w + (s + w)(2N - 1)$$

Therefore, the coil geometry can be derived from the last 2 equations for a certain desired inductance. The design process starts by selecting the value of  $D_o$ .  $D_o$  can be decided from the air-gap required between the primary and the secondary coil, as It has been established that the fundamental height of the flux path in a circular pad (or even circular Archimedean spiral) is about 25% of the coil diameter. Therefore, it gives an idea of how large the primary coil must be. If the air gap does not matter, then  $D_o$  can be decided from the available area on the place where the primary coil needs to be put. Once  $D_o$  is selected and “w” is calculated from the selected value of the current density for the coils, then we would get the value of “N” and “s” for every  $D_{in}$ .

It is obvious that we can obtain a series of coil geometry for the same L. This, in turn, leads to several primary and secondary coils for the given value of L. The coil-pair that is least affected by misalignment should be chosen for the SS-RIPT link.

#### 4.5.2. Mutual Inductance

After several pieces of research and revising many published papers it was found that the best way to achieve the needed mutual inductance between the two coils is experimentally by varying the air gap till achieving it.

## 5. Chapter 5: Designing a 500 W system

### 5.1. Calculation of Electrical Parameters

After understanding the procedures to calculate the electrical parameters of the system it is time to apply those equations on the desired system. For just validating the idea of RIPT with reasonable efficiency a small car model will be built, so the electrical parameters were calculated for 48 V output (battery pack) at 500 W and 40 kHz resonant frequency. Following the steps aforementioned, the parameters were calculated as follows:

#### 5.1.1. Secondary Side

$$R_o = \frac{V_o^2}{P_o} = \frac{48^2}{500} = 4.608 \Omega$$

$$R_L = \frac{8}{\pi^2} \cdot R_o = \frac{8}{\pi^2} \cdot 4.608 = 3.735 \Omega$$

$$V_{s-RMS} = 2\sqrt{2} \cdot \frac{V_o}{\pi} = 2\sqrt{2} \cdot \frac{48}{\pi} = 43.215 \text{ V.}$$

$$I_{s-RMS} = \frac{V_{s-RMS}}{R_L} = \frac{43.215}{3.735} = 11.57A.$$

$Q_s$  was selected to be 4, then  $L_s$  is given by:

$$L_s = \frac{Q_s \cdot R_L}{\omega} = \frac{4.3735}{2\pi \cdot 40000} = 59.44 \mu H.$$

$$C_s = \frac{1}{\omega^2 \times L_s} = \frac{1}{(2\pi \cdot 40000)^2 \times (59.44 \times 10^{-6})} = 266.34 nF$$

### 5.1.2. Primary Side

To increase the primary current hence decrease the needed mutual inductance it was decided to stepdown the grid voltage using 2:1 transformer before the rectifier so the that  $V_{P-RMS} = 110\sqrt{2}$  V.

$$I_{p-RMS} = \frac{P_o}{V_{P-RMS}} = \frac{500}{110\sqrt{2}} = 3.21 A.$$

$$M = \frac{R_L \cdot I_s}{I_p \cdot \omega} = \frac{3.735.11.57}{3.21.2\pi.40000} = 53.56 \mu H.$$

$$K_{cr} = \frac{1}{Q_s} \sqrt{1 - \frac{1}{4Q_s^2}} = \frac{1}{4} \sqrt{1 - \frac{1}{4 \cdot 4^2}} = 0.248.$$

As mentioned before, the coupling coefficient (K) must be less than  $K_{cr}$  so a value of 0.2 was chosen.

$$L_p = \frac{M^2}{L_s \cdot K^2} = \frac{53.56^2 \cdot 10^{-6}}{59.44 \cdot 0.2^2} = 1206.54 \mu H.$$

$$C_p = \frac{1}{\omega^2 \times L_p} = \frac{1}{(2\pi \cdot 40000)^2 \times (1206.54 \times 10^{-6})} = 13.12 nF$$

**Table (5.1)** summarizes all the calculated parameters

$V_{s-RMS}$	43.215 V
$I_{s-RMS}$	11.57 A
$L_s$	59.44 $\mu H$
$C_s$	266.34 nF
$V_{p-RMS}$	$110\sqrt{2}$ V
$I_{p-RMS}$	3.21 A
$M$	53.56 $\mu H$
$L_p$	1206.54 $\mu H$
$C_p$	13.12 nF

**Table 5. 1:** Electrical Parameters

## 5.2. Calculation of Geometric Parameters

After calculating the electrical parameters, it is time to design the geometry of the coil, inner diameter, outer diameter, number of turns, and the spacing of the turns. As mentioned before reaching the desired coil inductance can be done with many different designs and with different combinations, of primary and secondary coils. Five different coil-pair combinations were considered for finding the best one which is least sensitive to misalignment. The primary coil was kept unchanged in all five coil pairs. The coil pairs were as following:

1. Coil-pair P-S1: For this coil-pair, both the outer and the inner diameter of the primary and secondary coils are equal.

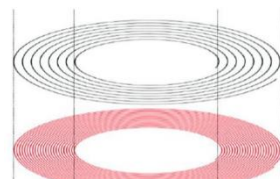


**Figure 5. 1:** Coil Pair P-S1

2. Coil-pair P-S2: For this coil-pair, the outer diameter of the secondary coil is less than the outer diameter of the primary coil and the inner diameter of the secondary coil is bigger than the inner diameter of the primary coil.

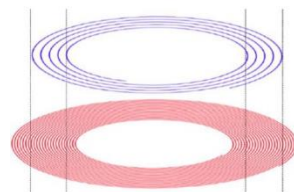


**Figure 5. 2:** Coil Pair P-S2

3. Coil-pair P-S3: For this coil-pair, both the outer diameter and the inner diameter of the secondary coil are smaller than the primary coil outer and inner diameters.

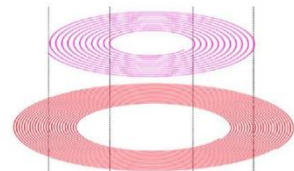


**Figure 5. 3:** Coil Pair P-S3

4. Coil-pair P-S4: For this coil-pair, the outer diameter of the secondary coil is equal to the outer diameter of the primary coil and the inner diameter of the secondary coil is larger than the inner diameter of the primary coil.

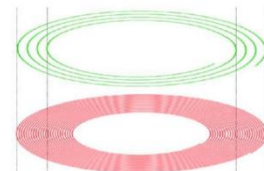


**Figure 5. 4:** Coil Pair P-S4

5. Coil-pair P-S5: For this coil-pair, the outer diameter of the secondary coil is less than the outer diameter of the primary coil and the inner diameter of the secondary coil is equal to the inner diameter of the primary coil.

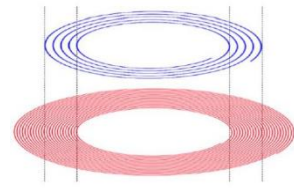


**Figure 5. 5:** Coil Pair P-S5

According to recent researches and experiments conducted on such combinations it was found that P-S4 is the best topology regarding the sensitivity to misalignment which means better performance while the vehicle's coil (secondary) is transferring between secondary coils on the road. Thus, the coils were fabricated according to that topology.

The outer diameter of both the primary and secondary coils ( $D_o$ ) was chosen to be 40 cm to fit in the model car and as mentioned before, the fundamental height of the flux path is approximately  $\frac{1}{4}$  of the coil's outer diameter and an air-gap of about 10 cm is anticipated.

### 5.2.1. Primary Coil

First, a suitable wire size should be chosen as follows:

$$\text{Wire area} = \frac{\text{Current (A)}}{\text{Current density } (\frac{\text{A}}{\text{mm}^2})} = \frac{4}{5} = 0.8 \text{ mm}^2$$

Where the current density is recommended to have a value that lies between 2 and 6 for a given continuous power level and temperature rise over ambient temperature for convection cooling.

Therefore, the wire diameter would be 1 mm and it was found that the overall diameter of the wire with the insulation is 2.2mm (w).

The next step was to construct a simple iteration table using EES program (or any other similar one) to choose the suitable inner diameter ( $D_i$ ) and number of turns (N) as shown in **figure (5.6)**:

The screenshot shows the EES software interface with the following data:

Run	Di	N	s
Run 1	0	95.88	-0.01263
Run 2	1	93	-0.01156
Run 3	2	90.25	-0.01074
Run 4	3	87.62	-0.01017
Run 5	4	85.11	-0.009858
Run 6	5	82.71	-0.0098
Run 7	6	80.41	-0.01
Run 8	7	78.2	-0.01048
Run 9	8	76.08	-0.01122
Run 10	9	74.05	-0.01225
Run 11	10	72.09	-0.01356
Run 12	11	70.21	-0.01516
Run 13	12	68.4	-0.01705
Run 14	13	66.65	-0.01925
Run 15	14	64.97	-0.02176
Run 16	15	63.34	-0.02458
Run 17	16	61.77	-0.02773
Run 18	17	60.25	-0.0312
Run 19	18	58.78	-0.03502
Run 20	19	57.35	-0.03918
Run 21	20	55.97	-0.04369
Run 22	21	54.63	-0.04857
Run 23	22	53.33	-0.05382
Run 24	23	52.07	-0.05946
Run 25	24	50.85	-0.06548
Run 26	25	49.66	-0.07191
Run 27	26	48.5	-0.07876
Run 28	27	47.38	-0.08604
Run 29	28	46.28	-0.09375
Run 30	29	45.21	-0.1019
Run 31	30	44.17	-0.1106

**Figure 5. 6:** Calculated Parameters on EES (Primary Coil)

### 5.2.2. Secondary Coil

$$\text{Wire area} = \frac{\text{Current (A)}}{\text{Current density } (\frac{A}{mm^2})} = \frac{15}{5} = 3 \text{ mm}^2$$

Therefore, the wire diameter would be 2 mm and it was found that the overall diameter of the wire with the insulation is 3.2mm (w).

The same steps were made like the primary coil taking into consideration that the inner diameter should be bigger than that of the primary coil. **Figure (5.7)** illustrates the chosen parameters.

Run	Di	N	L
Run 1	0	21.28	0.627
Run 2	1	20.64	0.6323
Run 3	2	20.03	0.6364
Run 4	3	19.45	0.6395
Run 5	4	18.89	0.6414
Run 6	5	18.36	0.6421
Run 7	6	17.85	0.6416
Run 8	7	17.36	0.6398
Run 9	8	16.89	0.6368
Run 10	9	16.44	0.6326
Run 11	10	16	0.627
Run 12	11	15.58	0.6201
Run 13	12	15.18	0.6118
Run 14	13	14.79	0.6021
Run 15	14	14.42	0.5909
Run 16	15	14.06	0.5783
Run 17	16	13.71	0.5642
Run 18	17	13.37	0.5485
Run 19	18	13.05	0.5313
Run 20	19	12.73	0.5124
Run 21	20	12.42	0.4919
Run 22	21	12.13	0.4696
Run 23	22	11.84	0.4456
Run 24	23	11.56	0.4197
Run 25	24	11.29	0.392
Run 26	25	11.02	0.3623
Run 27	26	10.77	0.3307
Run 28	27	10.52	0.297
Run 29	28	10.27	0.2612
Run 30	29	10.04	0.2232
Run 31	30	9.805	0.183

**Figure 5. 7:** Calculated Parameters on EES (Secondary Coil)

Since the coils were fabricated manually, the actual number of turns and spacings were not 100% exact, and therefore, there are some differences in the actual value of inductance especially in the primary coil that required 0.0 mm spacing between turns.

The final coils' parameters can be summarized in **table (5.2)**

Coil	D <sub>o</sub> (cm)	D <sub>i</sub> (cm)	N	S (cm)	W(cm)	L ( $\mu$ H) analytical	L ( $\mu$ H) measured	R ( $\Omega$ )
Primary	40	5	82	0	0.22	1206.54	960	4.93
Secondary	40	20	12.5	0.5	0.32	59.44	62.3	0.66

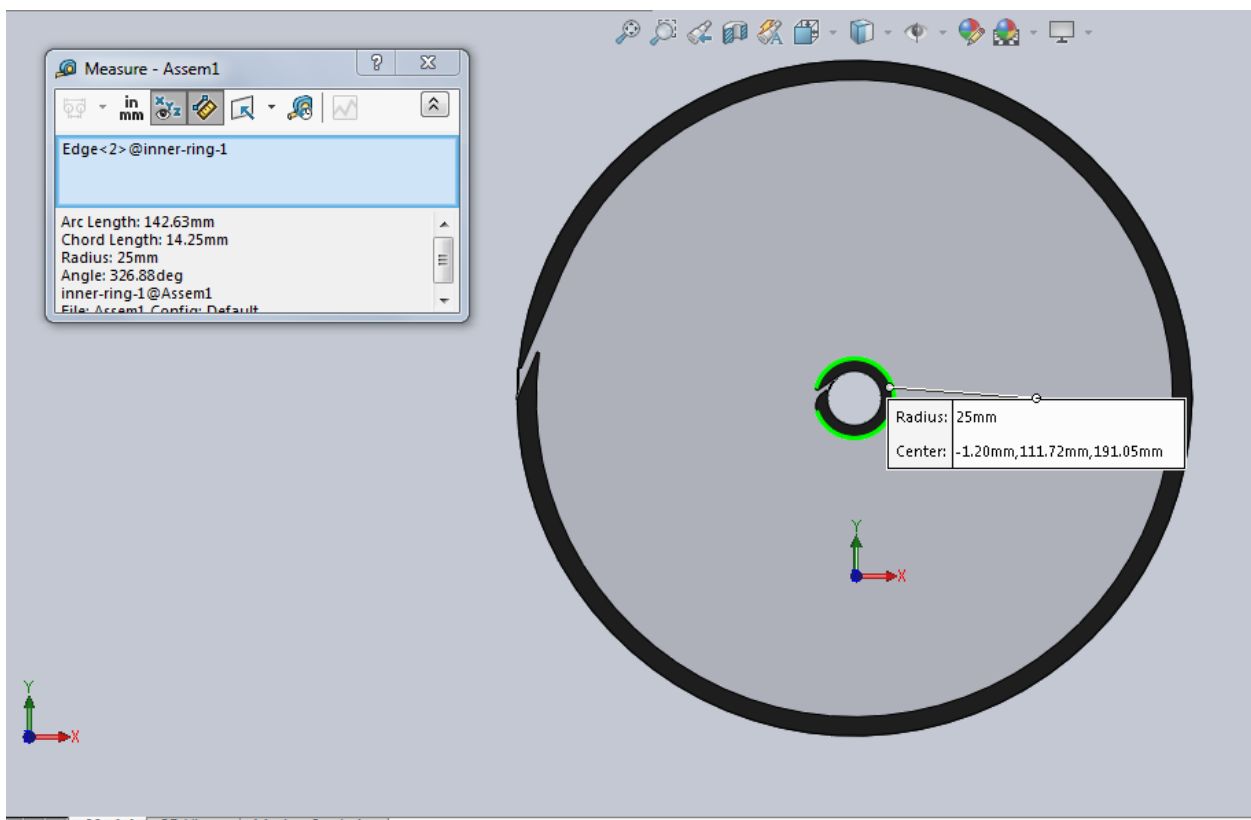
**Table 5. 2:** Coils' Final Parameters

### 5.3. Coil Manufacturing

Right after choosing the specifications of both the primary coil and the secondary coil, a challenge of creating a base holder for both coils was encountered.

The primary coil needed to have zero spacing within its swirly shape along with inner and outer boundaries, whilst the secondary coil needed to have a considerable constant space between each turn along with inner and outer boundaries as well. These restrictions were inevitable for improving the efficiency of the wireless transmission.

The dimensions below of both the primary **figure (5.8)** and secondary **figure (5.9)** coils are based on the previous calculations.



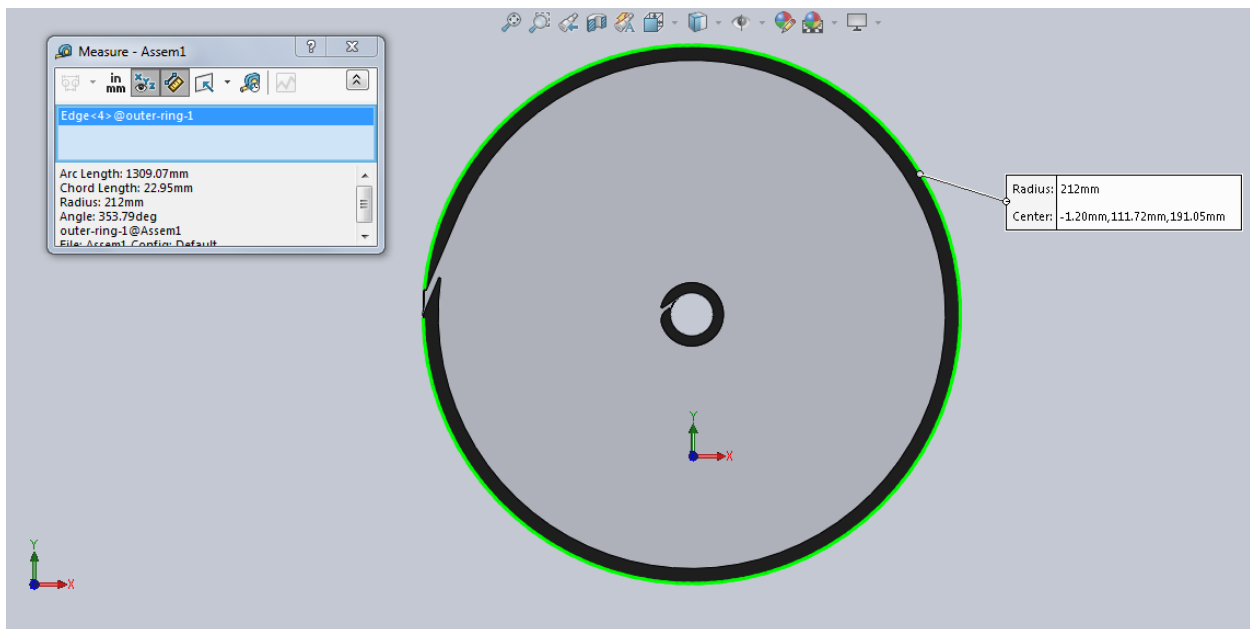
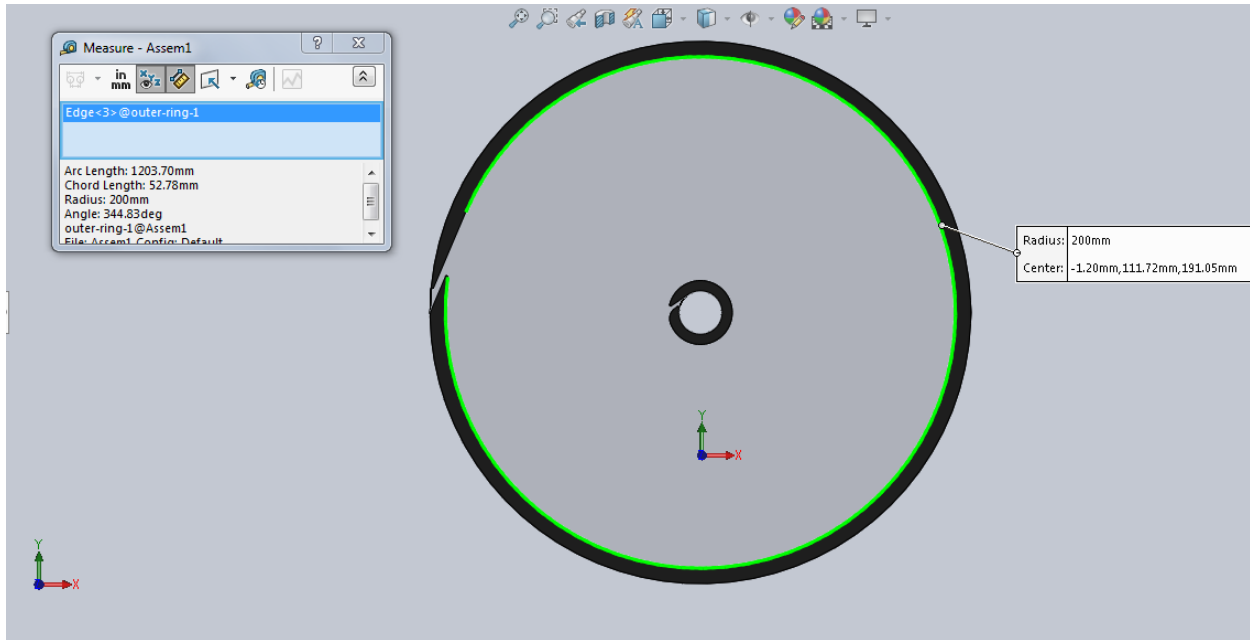


**Figure 5. 8:** Primary Coil Base Dimensions

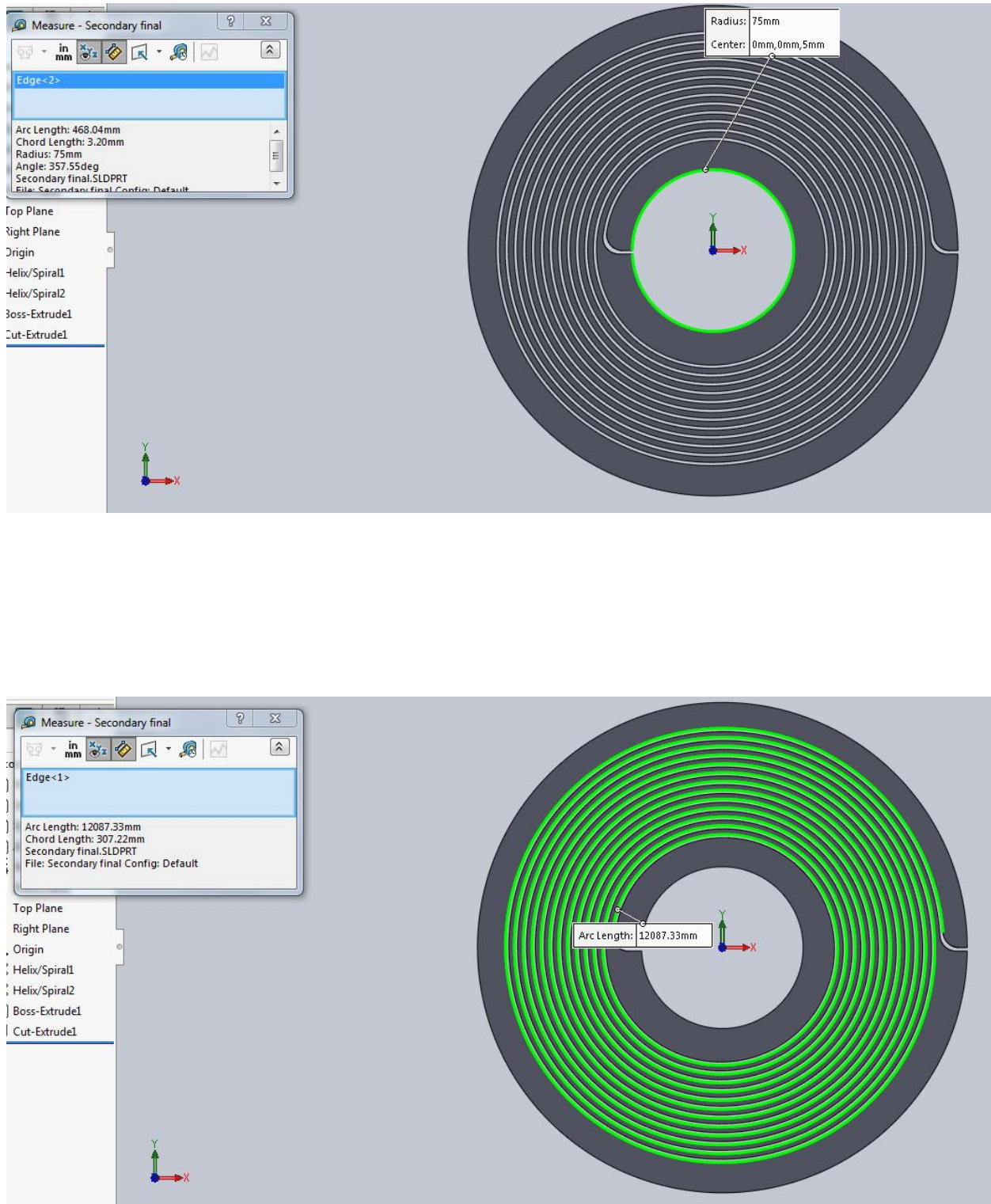


**Figure 5.9:** Secondary Coil Base Dimensions

Now, that the SOLIDWORKS models were implemented, a material should be chosen for both bases. At the beginning, wood was preferred due to its low cost and its availability, However the main problem was its flexibility specially in the secondary base due to its great cuts along its design on the same volume. Later on, Acrylic material was used due to its rigidity although it was considerably expensive. In the **figure (5.10)** and **figure (5.11)** shows the primary and secondary coils after manufacturing:



**Figure 5. 10:** Primary Coil

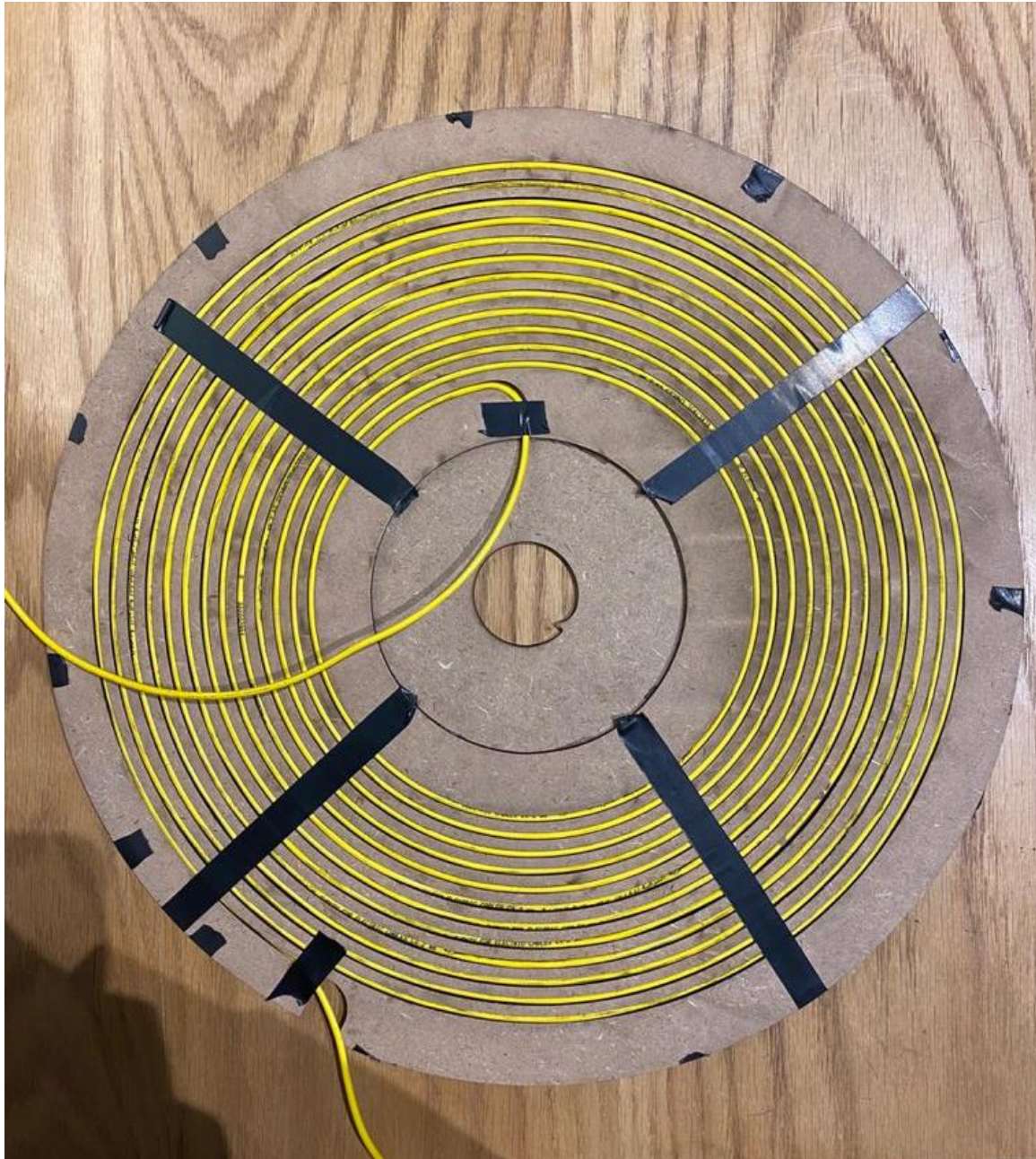


**Figure 5. 11:** Secondary Coil

#### 5.4. Ferrite Addition

Following the coil manufacture, it was essential to add a layer of ferrite to both primary and secondary coils -as shown in **figure (5.12)**- that would aid in proper direction of the produced magnetic field lines and creating a high-density magnetic field increasing the entire system efficiency.

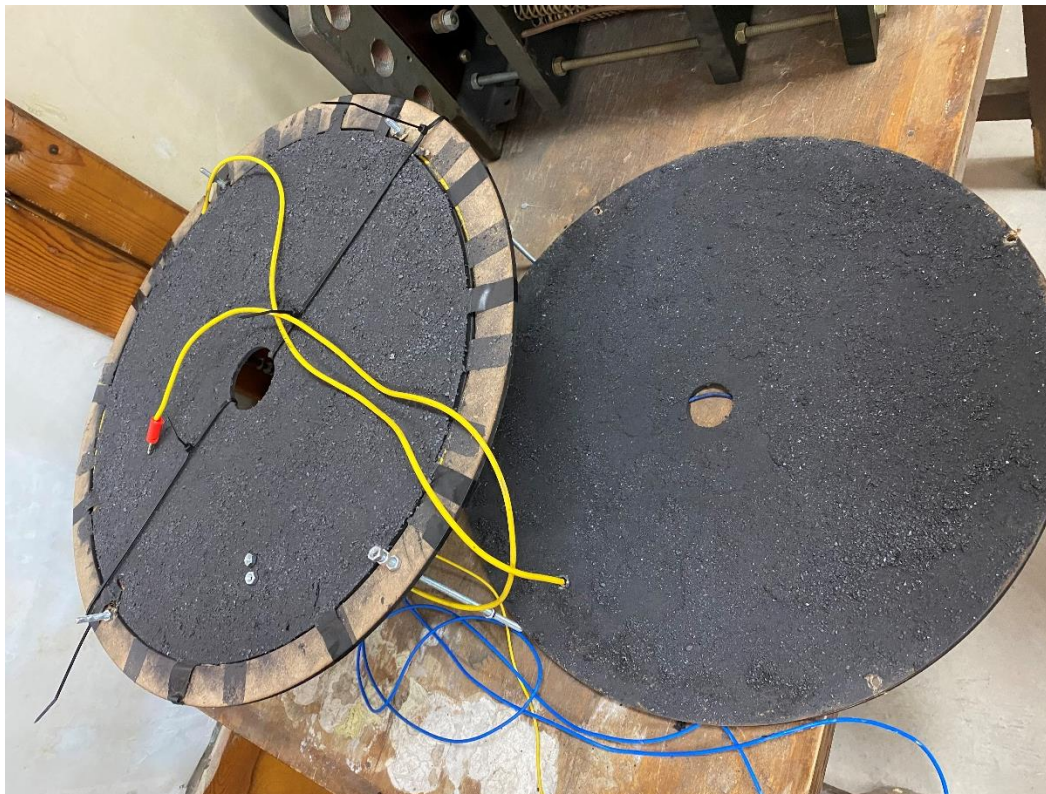


**Figure 5. 12:** Primary and Secondary Coils After Adding Ferrite Layer

## 6. Chapter 6: Simulation Results

In this chapter, the resonant inductive wireless power transmission system is simulated on MATLAB based on the components' values stated before in the paper using both MATLAB PowerSys and Simscape.

### A. MATLAB PowerSys

Firstly, the basic system will be introduced which consists of only one primary coil and a secondary coil as shown in **figure (6.1)**.

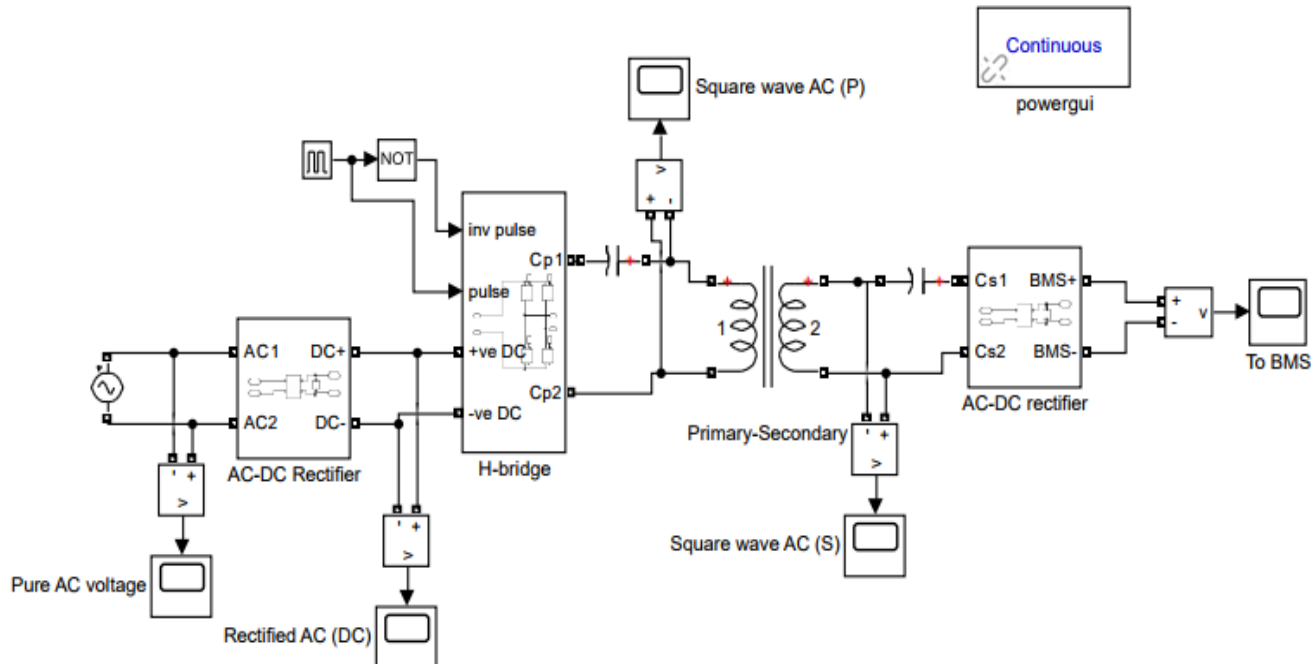


**Figure 6. 1: Basic System**

By splitting each component in the previous circuit:

### 6.1. AC-DC Rectifier

This, in fact, is responsible for the rectification of the AC voltage obtained from the grid to an almost pure DC wave shown in **figure (6.2)**. The impurities found in the shape of ripples is a factor of the components' efficiencies.

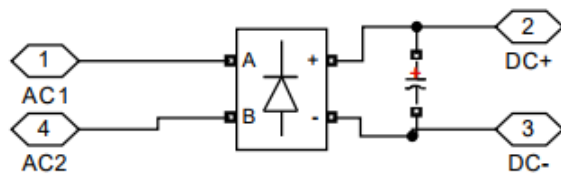


**Figure 6. 2: AC-DC Rectifier**

#### 6.1.1. Terminals

- **AC1, AC2** are connected to terminals of the AC voltage supply grid.
- **DC+, DC-** are connected to terminals of H-bridge.

#### 6.1.2. Parameters

Parameter	Value
Branch type	C
Capacitance C (F)	10e-3

#### 6.1.3. Components

- Universal Bridge:
  - 4 Diodes
- Capacitor

## 6.2. H-Bridge

The H-bridge is responsible for converting the DC wave into a high-frequency AC wave shown in **figure (6.3)** (almost 40 kHz frequency assuming that it is the resonant frequency).

Gating signals from a microcontroller are responsible for the emission of pulses equivalent to switching MOSFETS ON and OFF and eventually creating the high Ac frequency voltage.

In this MATLAB simulation, it is resembled as pulses with a given time interval without digging underneath the hood to how those signals were produced. Microcontroller circuit and gating signals are explained extensively previously.

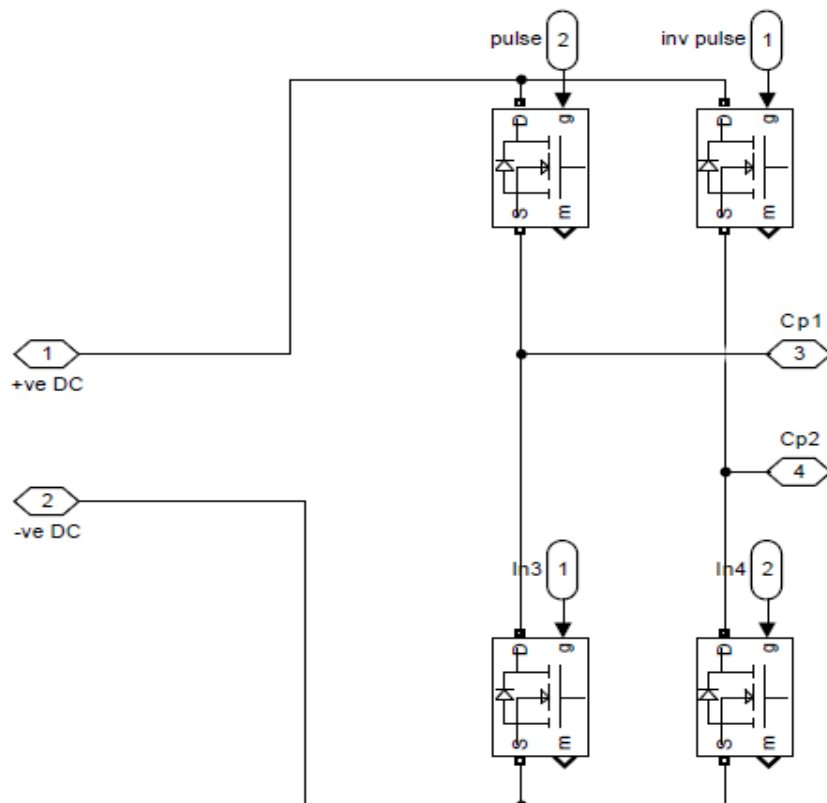


**Figure 6. 3: H-Bridge**

### 6.2.1. Components

- 4 Power MOSFETs

### 6.2.2. Terminals

- +ve DC, -ve DC are connected to terminals of rectified DC voltage obtained previously.
- Pulse, In3 are connected practically to HO, LO terminals of the IR driver.
- Inv pulse, In4 are connected practically to HO, LO terminals of the 2<sup>nd</sup> IR driver.

### 6.2.3. Parameters

Parameter	Value
Branch type	C
Capacitance C (F)	10e-3

### 6.3. Primary and Secondary Coils

The primary and secondary coils were resembled as a linear transformer as shown in **figure (6.4)**.

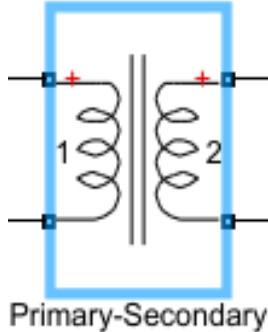


**Figure 6. 4:** Primary-Secondary Coils

#### 6.3.1. Coils Parameters

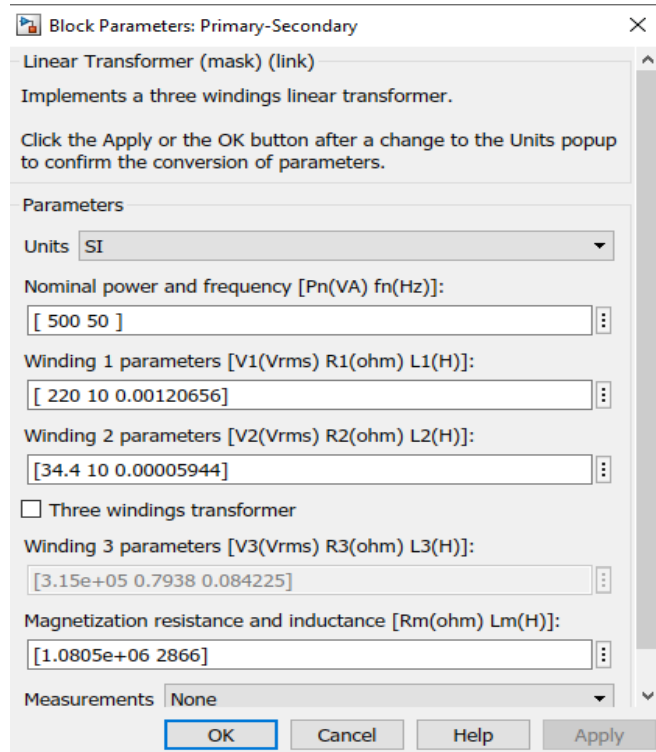


**Figure 6. 5:** Coils Parameters

## 6.4. AC-DC Rectifier

This is the second AC-DC rectifier -shown in **figure (6.6)** - in the circuit which is located on the secondary side of the system (car's side).

It is responsible for converting the absorbed AC voltage from the secondary coil to a DC voltage to be supplied to the BMS (Battery Management System).

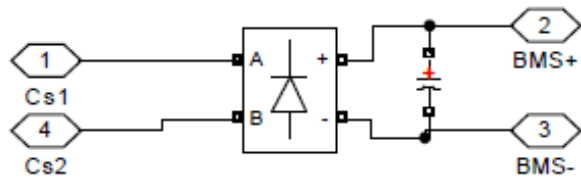


**Figure 6. 6:** AC-DC Rectifier

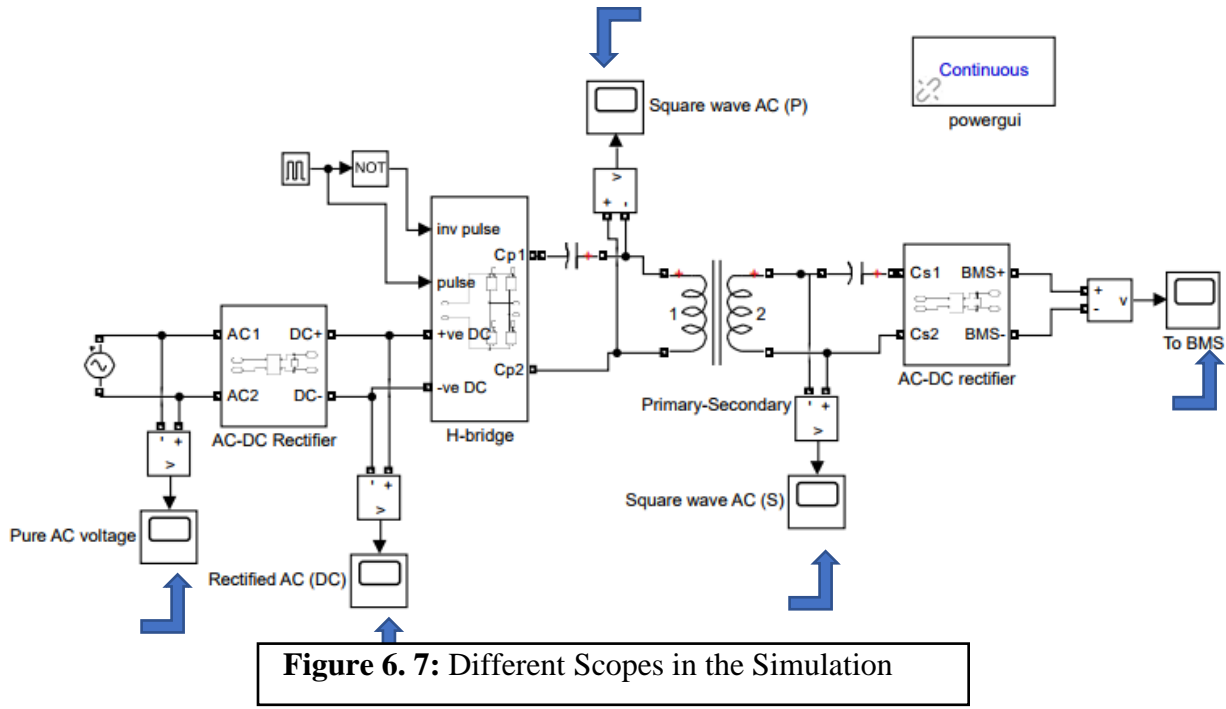
### 6.4.1. Terminals

- **Cs1, Cs2** are connected to terminals of the secondary coil.
- **BMS+, BMS-** are connected to terminals of the BMS.

### 6.4.2. Parameters

Parameter	Value
Branch type	C
Capacitance C (F)	10e-3

Next, each scope in the circuit as shown in **figure (6.7)** will be discussed in detail to output the simulation of the whole system.



## 6.5. Pure AC voltage Scope

### 6.5.1. Scope Output

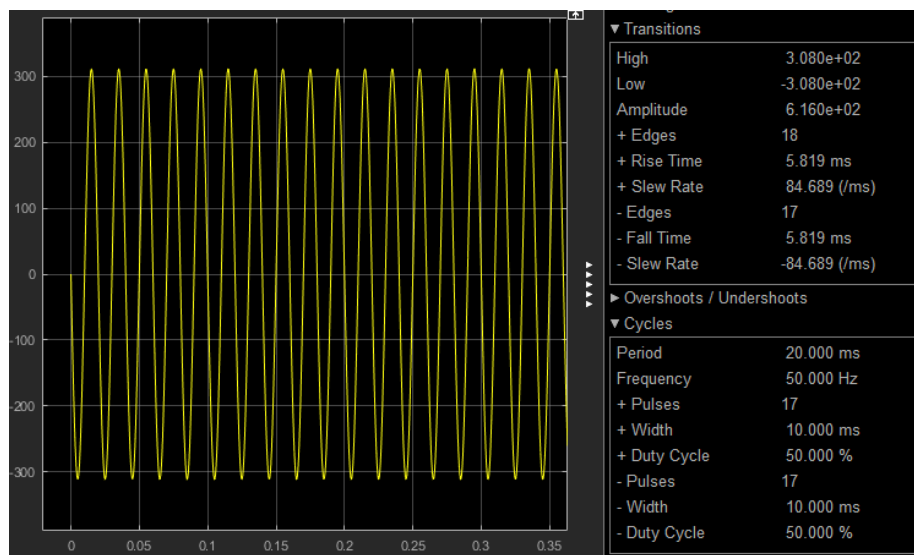


**Figure 6.8: Pure AC Voltage Scope Output**

### 6.5.2. Parameters:

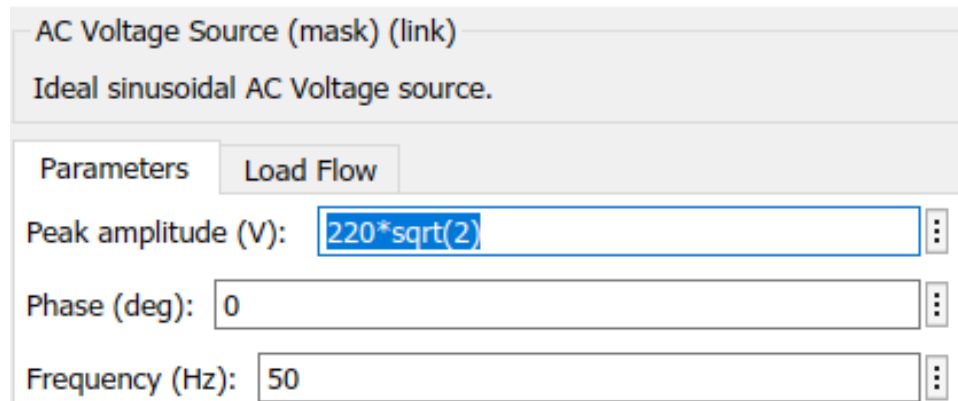


**Figure 6. 9:** Pure AC Voltage Scope Parameters

## 6.6. Rectified AC (DC) Scope

### 6.6.1. Scope Output

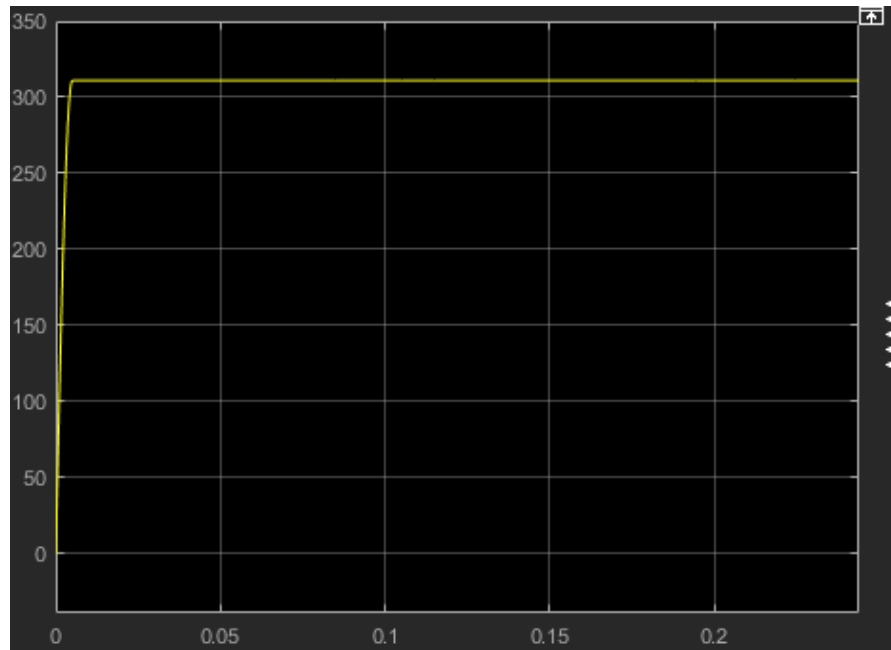


**Figure 6. 10:** Rectified AC (DC) Scope Output

\*This is a pure DC wave resulting from the AC-DC rectification process reaching a peak value of  $220\sqrt{2}V$ .

## 6.7. Square wave AC (P) Scope (Primary Voltage)

### 6.7.1. Scope Output

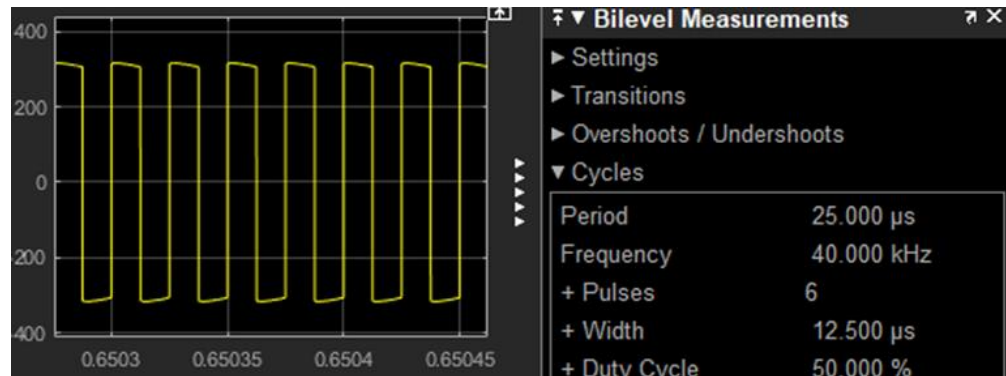


**Figure 6. 11:** Square wave AC (P) Scope Output

## 6.8. Primary Current

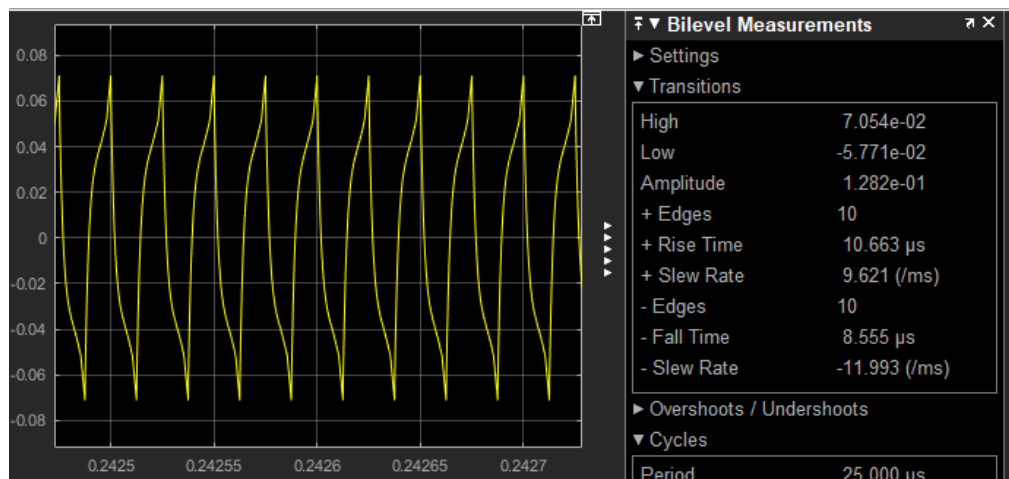


**Figure 6. 12:** Primary Current

## 6.9. Square wave AC (S) Scope (Secondary Voltage)

### 6.9.1. Scope Output

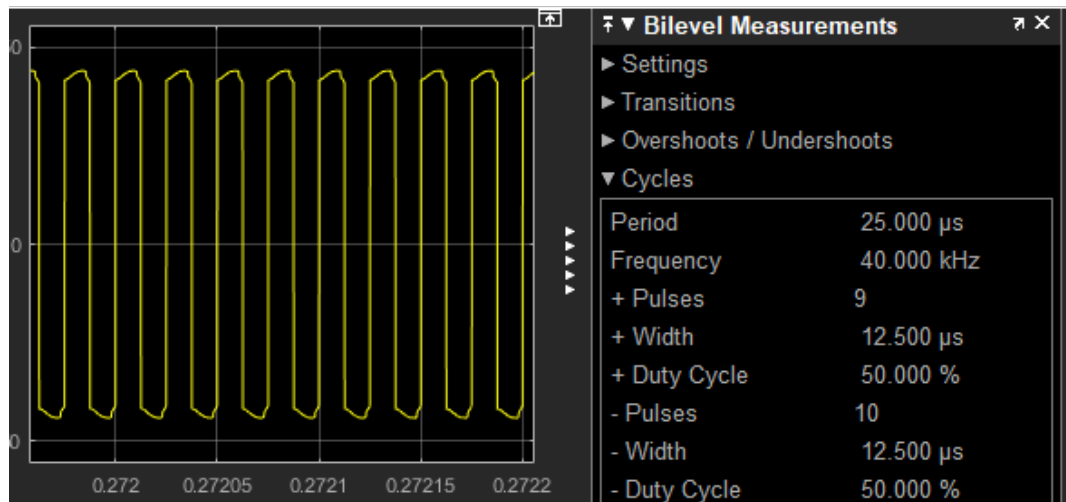


**Figure 6. 13:** Square wave AC (S) Output

## 6.10. Secondary current

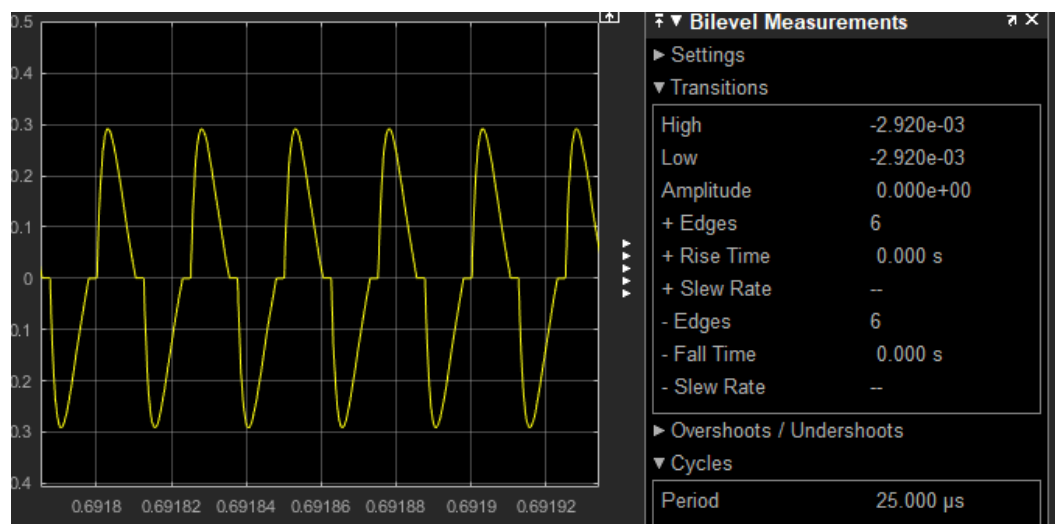


**Figure 6. 14:** Secondary Current

Note:

Due to different windings of the primary and secondary coil, which is resembled in the simulation as a linear transformer, voltage level decreased from 300v to almost 50v.

### 6.11. To BMS Scope:

#### 6.11.1. Scope Output

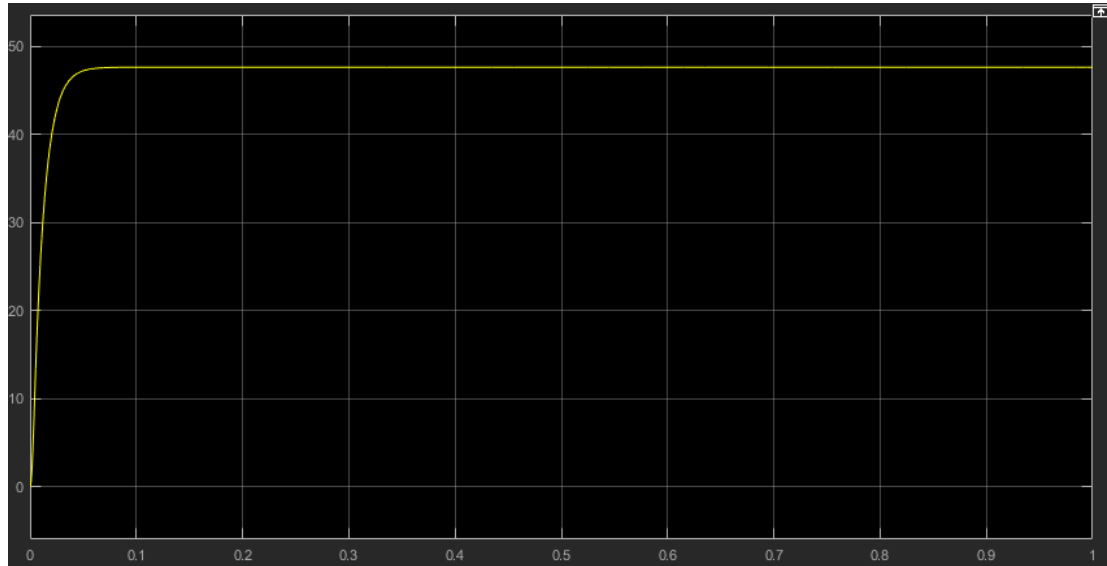


**Figure 6. 15:** To BMS Scope Output

\*Voltage level of nearly 48v is fed to the BMS at the end of the process.

## B. MATLAB SimScape

The previously mentioned circuit was fully explained using PowerSys libraries in MATLAB, however, further investigations required resembling the system in SimScape in order to approach practical results. Shown below **figure (6.14)** the full circuit using SimScape:

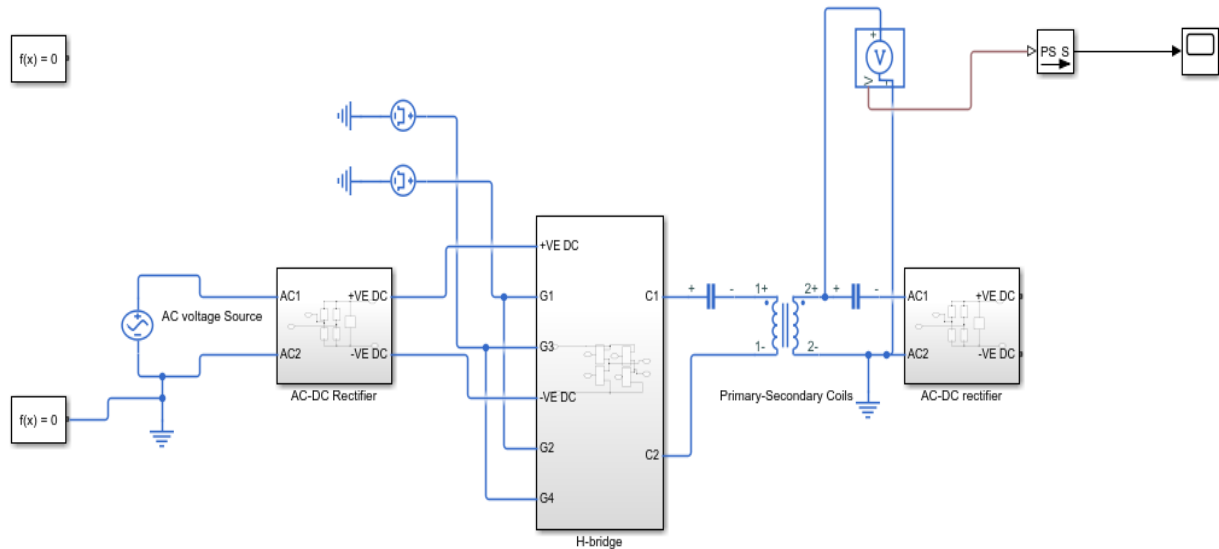


**Figure 6. 16:** Full Circuit Using SimScape

Performing the simulation in the SimScape program was one of the main challenges due to the fact of using sophisticated equations which either led to more errors in the simulation or the program itself crashing.

Further implementations were added in the PowerSys mode which was much easier than implementing the same methods in SimScape.

Shown below in **figure (6.15)** the full implementation of the MATLAB simulation using two primary coils being connected to one secondary coil (resembling the car) in sequence

This system is just a brief picture of how the system should behave. The system shown may differ slightly from the practical system.

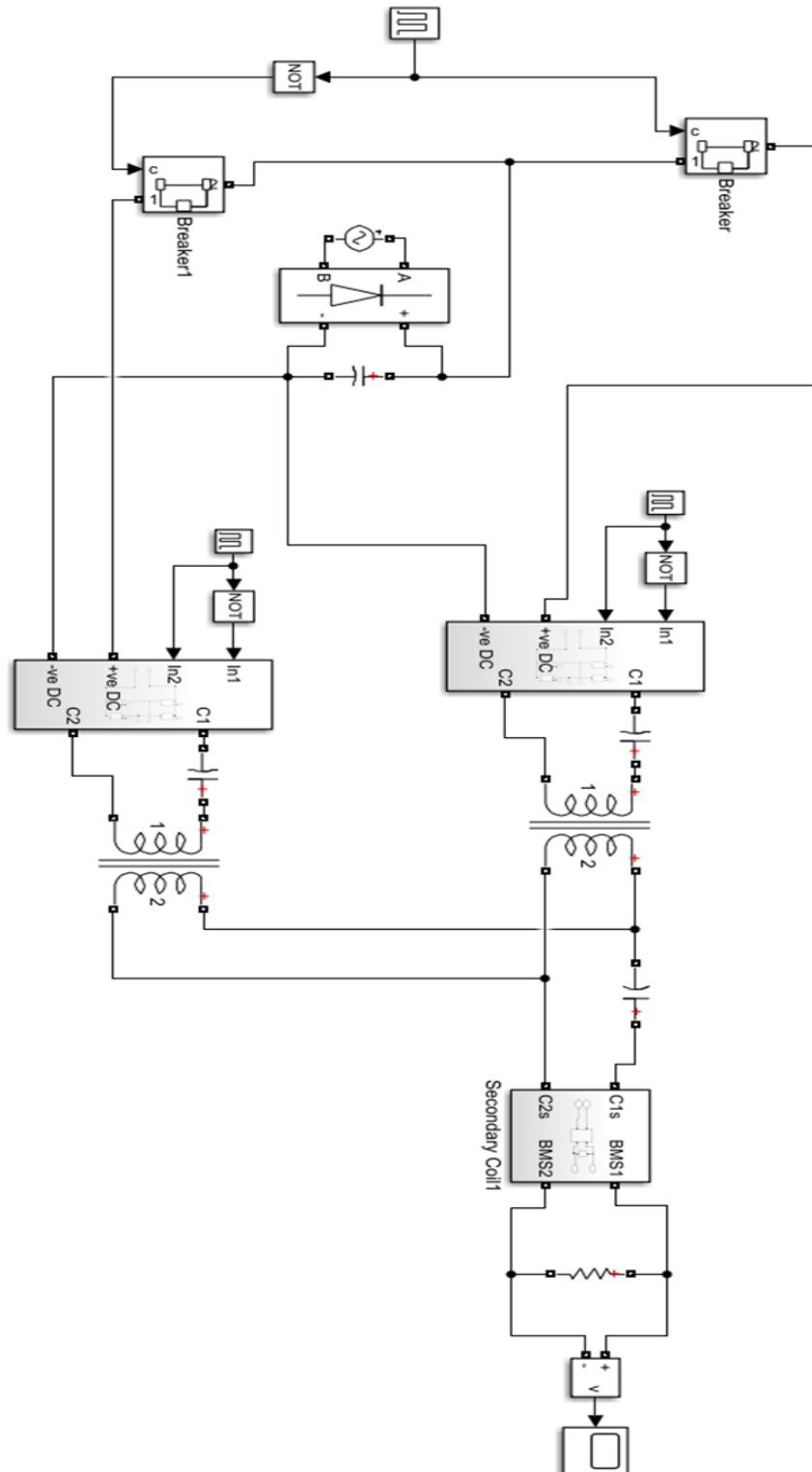


**Figure 6. 17:** Full Implementation of Both MATLAB Simulation and Practical Sensors

- Proximity sensors detect an EV passing by, thus connecting both primary circuits of the 2 primary coils. Proximity sensors are to be connected via relay circuits to the primary circuit as shown in **figure (6.16)**.

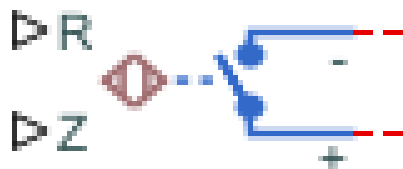


**Figure 6. 18:** Relay Circuit

### C. Proteus Simulation

The primary coil and H-bridge were simulated using proteus to assess the resulting waves, and upon, indicating the presence of a square wave voltage and consequently a sine wave current due to the effect of inductance in the circuit.

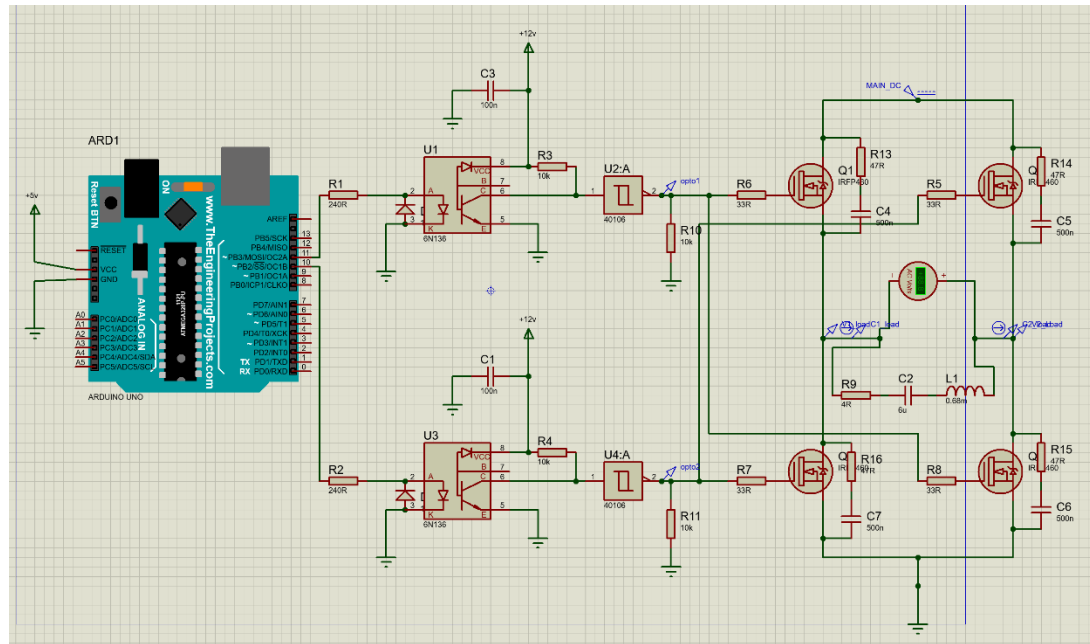


**Figure 6. 19:** Proteus Simulation



**Figure 6. 20:** Primary Voltage and Current

## D. Closed Loop Control

The closed loop control for our system as shown in **figure (6.21)** controls the frequency, it needs to ensure zero phase shift between voltage and current to any connected RLC load which represents the coil and compensating capacitors connected to the controller.

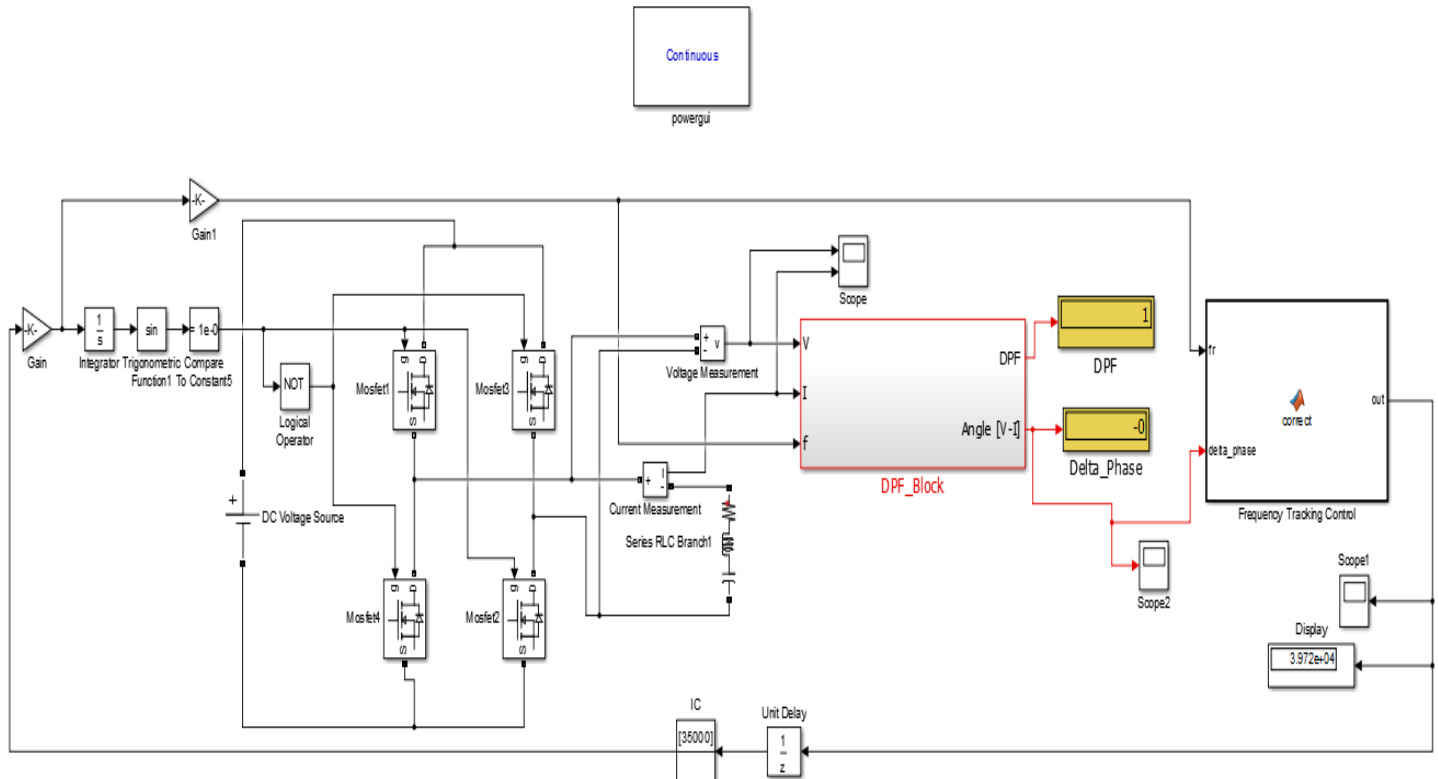


**Figure 6. 21:** Feedback Control System

The proposed control uses the rectified output of the system (half-wave rectification) and attaches an interrupt routine on both rising and falling edges for the current signal, when an interrupt occurs the voltage signal value is checked, if voltage is high with current's rising edge then the system lags and frequency needs to be decreased, while if voltage is high during a falling edge interrupt then the system leads and frequency needs to be increased to achieve a unity power factor with no reactive power losses.

The system as proposed was to be implemented through the AVR (ATmega32) microcontroller already used to generate gate signals at desired frequency, but the system was simulated on MATLAB Simulink.

The MATLAB Simulink simulation controls the frequency using a MATLAB function (frequency tracking control) which takes system frequency and phase shift as inputs, performs the frequency control through a C code nearly the same as the one that would have been written for the microcontrollers, then outputs a new frequency value which brings the system closer to resonance. Both the system's initial frequency value and frequency change step can be controlled easily through two variables in the beginning of the code.

## 6.12. MATLAB Function

```
function out = correct(fr, delta_phase)
step = 0.005;
initcond = 35000;
perfect = 0;

if perfect == 0

if (delta_phase > 0)
    out=fr+step;

elseif (delta_phase < 0)
    out=fr-step;

elseif delta_phase == 0
    perfect = fr;
    out = perfect;
else
    out = initcond;
end

else
    out = perfect;
end
```

### 6.13. System Frequency

**Figure (6.22)** shows how the frequency is varied till reaching resonance condition.

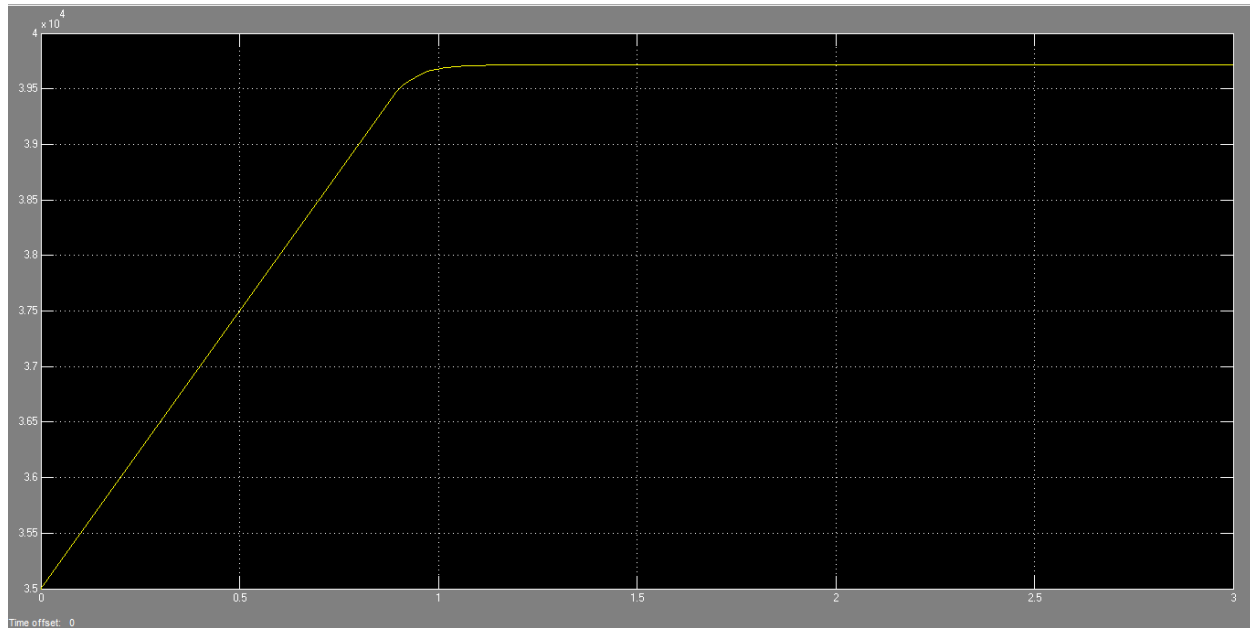


**Figure 6. 22:** Frequency Variation

### 6.14. System Before Control

At the beginning of the operation the frequency was adjusted to 35 kHz which results in the current leading the voltage as shown in **figure (6.23)**,

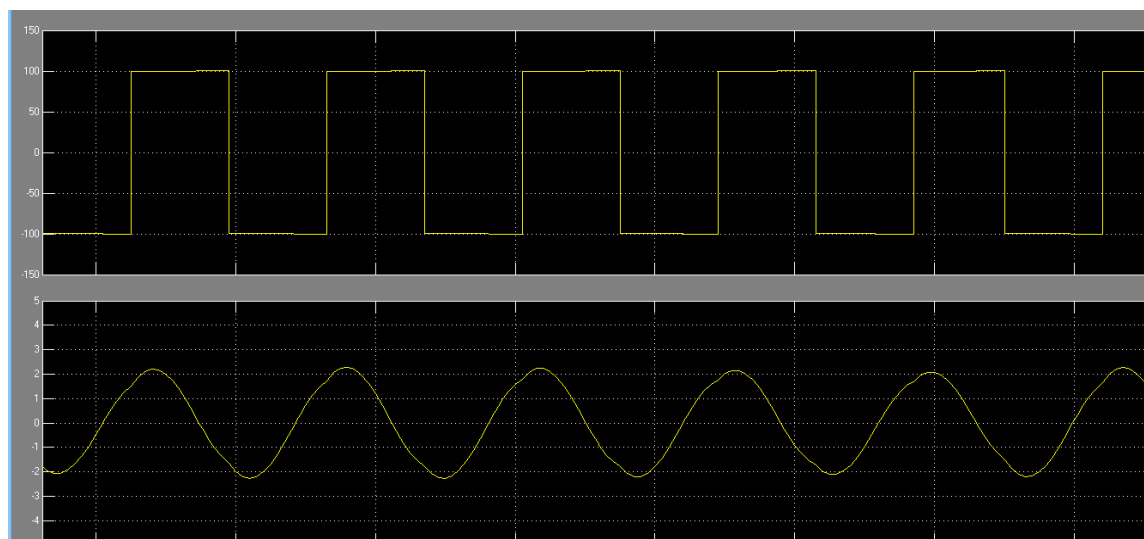


**Figure 6. 23:** Initial Voltage & Current

## 6.15. System at Steady State

As the frequency starts to increase steadily, the phase angle starts to decrease until reaching zero where perfect resonance is achieved as shown in **figure (6.24)**.

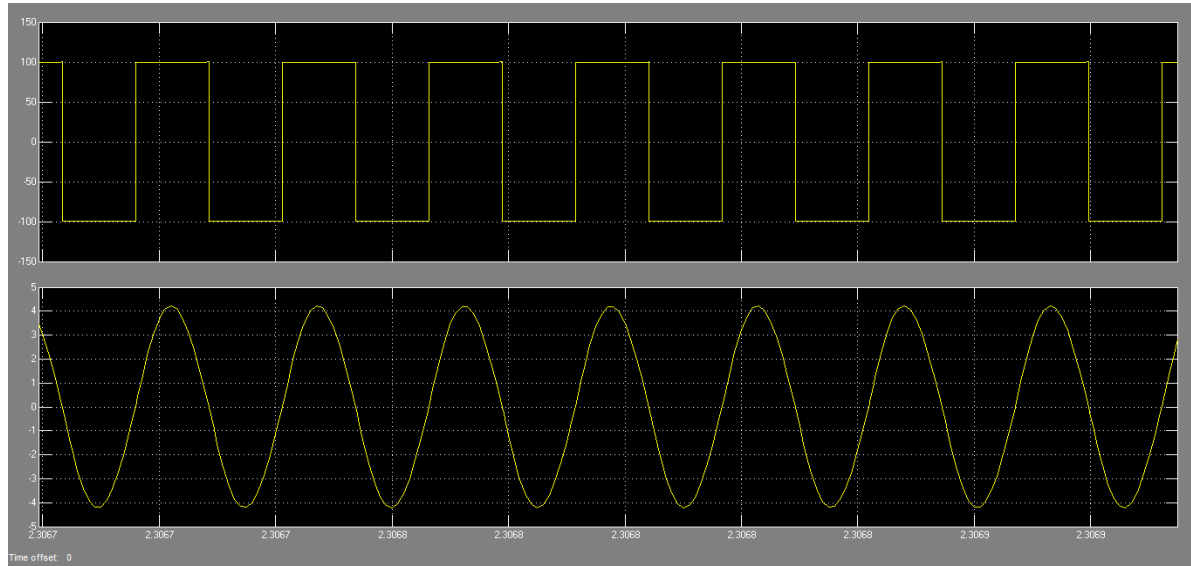


**Figure 6. 24:** Voltage & Current at Zero Phase Shift

## 6.16. Measuring Phase Shift

**Figure (6.25)** shows the change in the phase shift between both the voltage and the current till reaching its steady state with zero phase shift.

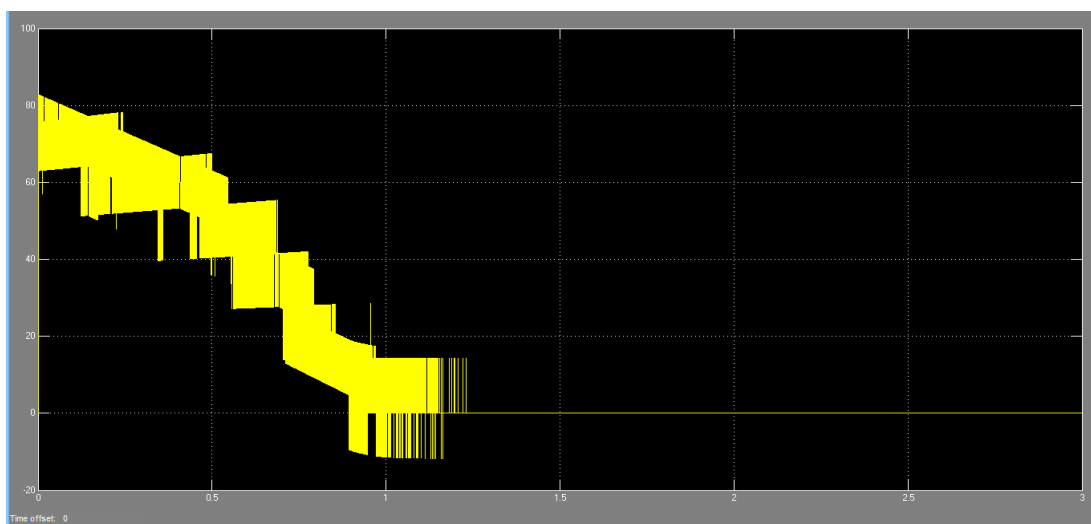


**Figure 6. 25:** Phase Shift Variation

## 7. Chapter 7: Experimental Setup and Results

### 7.1. Testing:

Testing is mandatory to assess the current charging system, and to maintain a proper evaluation of its performance. Tests were to be implemented in 2 phases. First phase is static testing, while the second phase is dynamic testing. Due to lack of time, only static tests were run while dynamic tests were suggested to be a mandatory phase in future improvements before a final release of the project.

#### 7.1.1. Static Testing

A certain mechanism- as shown in **figure (7.1)**- was engineered to sustain a proper testing of the charging system ensuring exact alignment and centralization of both primary and secondary coils and offering a free vertical movement to adjust the air gap distance under desired conditions using a power screw.

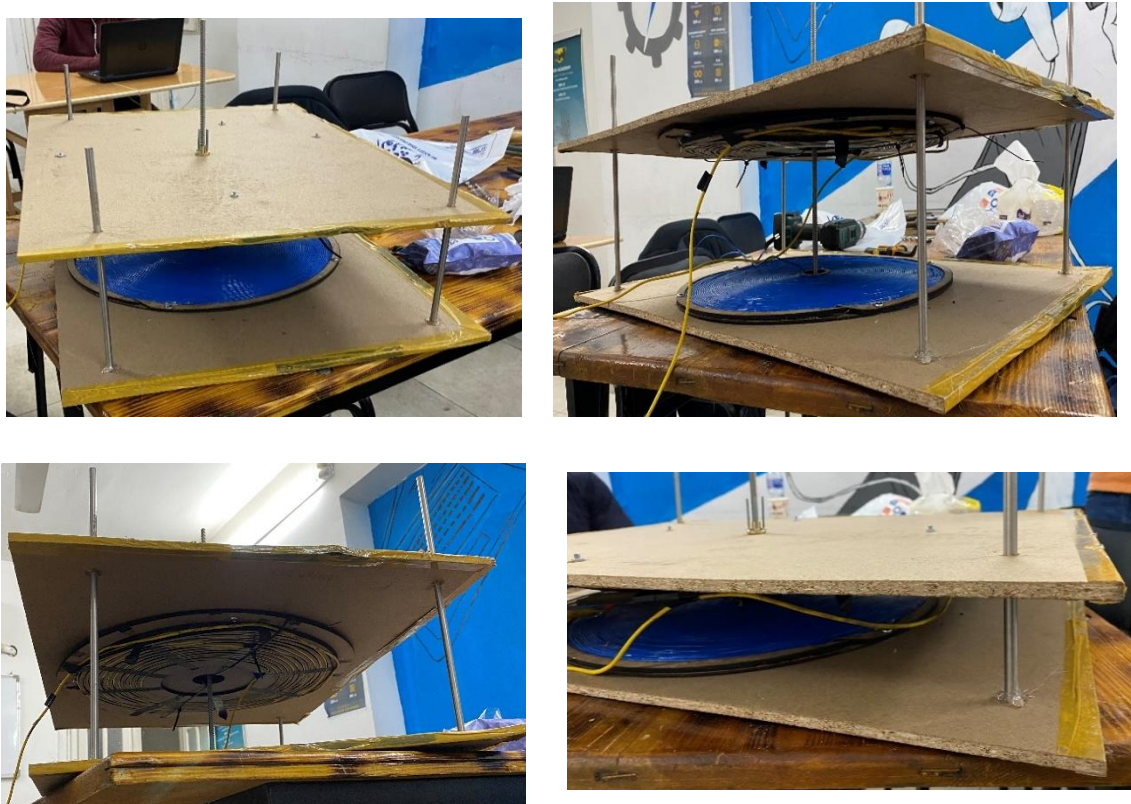


**Figure 7. 1:** Testing Mechanism

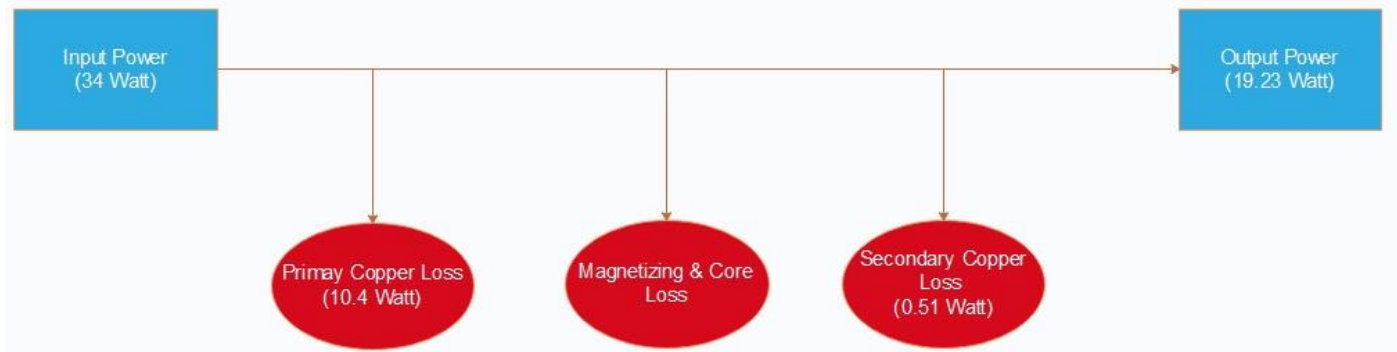
Tests were run in static mode maintaining an air gap between the primary and secondary coils while both being concentric and parallel to each other.

Using an oscilloscope and a current meter the following readings were obtained.

### 1. 7 cm air gap:

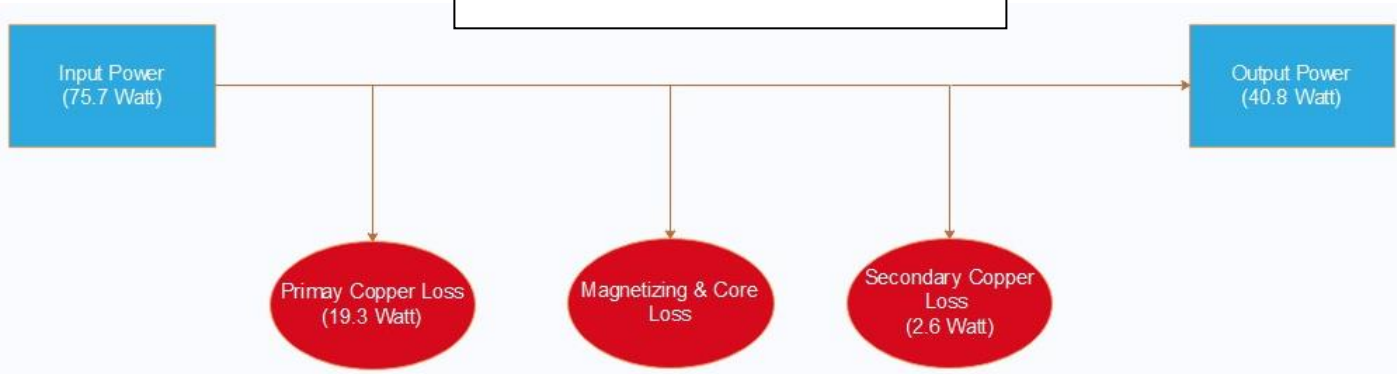
Coil	Voltage (v)	Current (A)	Phase-Shift (Degrees)	Power (Watt)	Copper Loss (Watt)	Percentage of Copper Loss	Efficiency
Primary	40	1.45	54	34	$(1.45)^2 \times 4.93 = 10.4$	32.1 %	56.6 %
Secondary	70.7	0.88	72	19.23	$(0.88)^2 \times 0.66 = 0.51$		

**Table 7. 1:** Testing at 40 Input Voltage



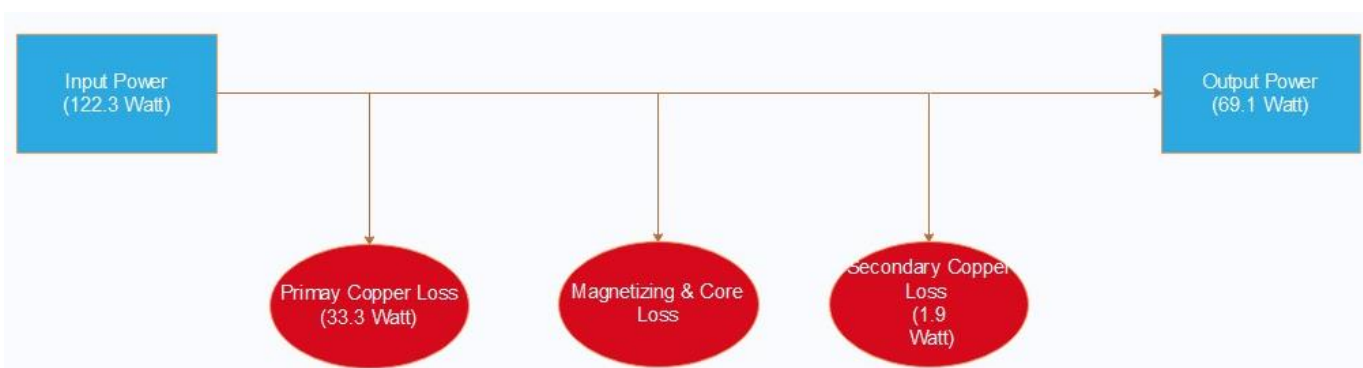
Coil	Voltage (v)	Current (A)	Phase-Shift (Degrees)	Power (Watt)	Copper Loss (Watt)	Percentage of Copper Loss	Efficiency
Primary	60	1.98	50.4	75.7	$(1.98)^2 \times 4.93 = 19.3$	28.9 %	53.9 %
Secondary	103.94	1.27	72	40.8	$(1.27)^2 \times 0.66 = 2.6$		

Table 7. 2: Testing at 60 Input Voltage



Coil	Voltage (v)	Current (A)	Phase-Shift (Degrees)	Power (Watt)	Copper Loss (Watt)	Percentage of Copper Loss	Efficiency
Primary	80	2.6	54	122.3	$(2.6)^2 \times 4.93 = 33.3$	27.9 %	56.5 %
Secondary	132.35	1.69	72	69.1	$(1.69)^2 \times 0.66 = 1.9$		

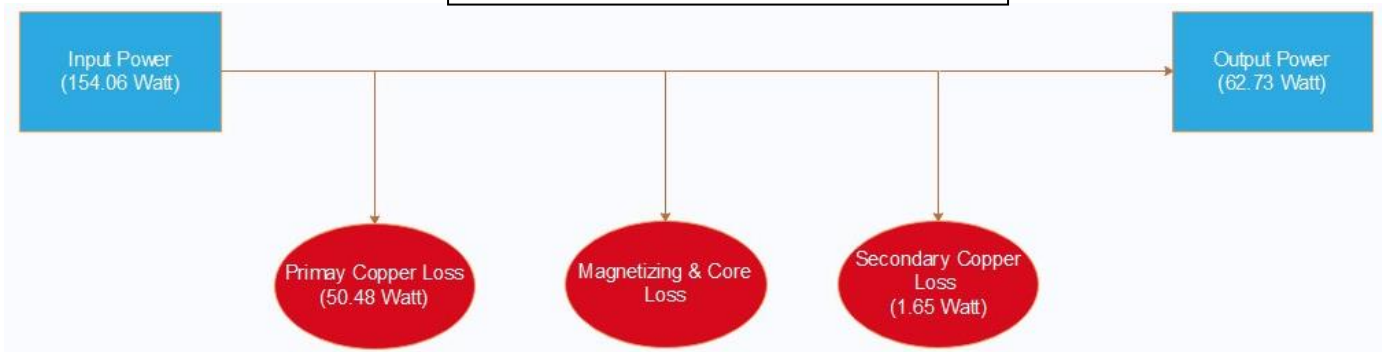
Table 7. 3: Testing at 80 Input Voltage



## 2. 10 cm air gap:

Coil	Voltage (v)	Current (A)	Phase-Shift (Degrees)	Power (Watt)	Copper Loss (Watt)	Percentage of Copper Loss	Efficiency
Primary	80	3.2	53	154.06	$(3.2)^2 \times 4.93 = 50.48$	33.84%	40.7 %
Secondary	128.5	1.58	72	62.73	$(1.58)^2 \times 0.66 = 1.65$		

**Table 7. 4:** Testing at 80 Input Voltage



The following graphs were obtained using an oscilloscope:

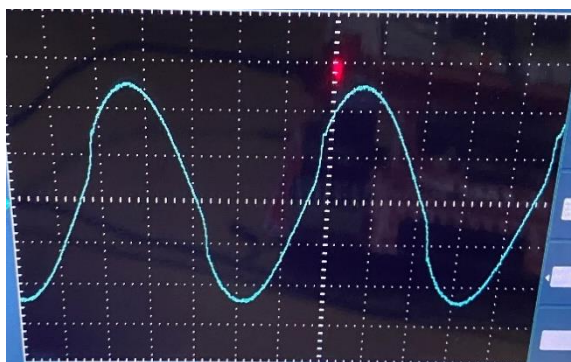


**Figure 7. 3:** Primary Current

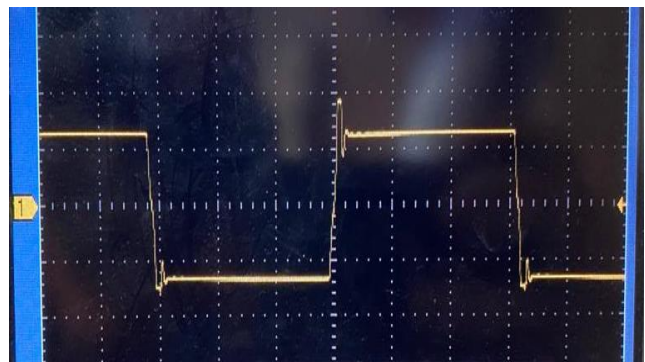


**Figure 7. 2:** Primary Voltage

- **Note:**

- 1) The power calculations did include a phase shift that was not accounted for prior to testing due to some error in calculating the compensating capacitors that would maintain a zero-degrees phase shift.
- 2) Notice the decrease in efficiency as the air gap increases indicating an inverse proportional relation between both parameters.

## 8. Chapter 8: Future Improvements:

### 8.1.1. Dynamic Testing

In order to finish the evaluation process and reach the end results of the project, dynamic testing operations shall be implemented using the suitable apparatus and proper tools. Such tests would be helpful with efficiency calculations and recording the entire system data sheet.

Dynamic tests would simulate the dynamic charging of an EV on road revealing important data such as; the charge rate of a battery, the dynamic power transmission efficiency and the effect of relative movement between the primary and receiver coils on the diminishing magnetic field in between, and upon, the system drawbacks shall be concluded and consequently system enhancements and related procedures shall be implemented to ensure a more efficient system.

### 8.1.2. Feedback Control

In order to achieve a power factor of 1 and get rid of any reactive power, a feedback control system was suggested to be implemented using sensors to detect zero-crossing of both primary voltage and current values, and upon, the actual phase shift will be used to calculate an exact suitable system frequency that would aid to achieve a phase shift of zero so as to reach the maximum true power available reducing power loss and therefore obtain a better system efficiency.

### 8.1.3. System Synchronization

The system being held with multiple primary coils and only one receiver (assuming one vehicle on road for simplicity), using the system inverters to supply continuous power to primary coils from the grid at all times will lead to a significant power loss, instead, the idea of ‘System Synchronization’ was introduced to the system.

The road will be mounted by proper sensors that would allow to detect the presence of a vehicle within a proper distance from a primary coil and using a suitable configuration, certain primary coils shall be activated to transmit power to the receiver in motion while the other primary coils are in rest position.

One inverter shall be used to power 2 to 3 primary coils simultaneously to ensure a dense magnetic field opposing the vehicle's receiver plate.

#### 8.1.4. Coil Geometry

It was discussed before that the coil geometry has a significant effect to the shape of the resulting magnetic field and how that shall enhance power transmission between coils and accordingly a more complex geometry would better be used instead of the current default circular shape which was implemented due to its simplicity and feasibility.

#### 8.1.5. Litz Wire

It was suggested to use Litz Wire instead of copper wire due to better characteristics that shall increase the system efficiency.

#### 8.1.6. Ferrite Material

It was found that a proper configuration of shaped ferrite plates would enhance power transmission, and detailed calculations would help analyze the magnetization effect, and upon, decrease the power loss.

## 9. Chapter 9: Financial Analysis

Through the financial section two major parts will be discussed, first part is the cost of the static system prototype. Second part is an estimation for the price per kilometer per lane for a dynamic system which plays a huge role in the decision whether to start such a project or not and whether it is feasible or not.

### 9.1. Prototype

The prototype used in this project wasn't the best yet it was enough to prove theory at acceptable conditions, more modification can be made which will furthermore increase the efficiency of the system, most of those modifications were discussed previously through the future improvements section.

Also as previously discussed the system consists of a number of crucial components needed to establish a wireless power transfer system. These components are all mentioned in **table (8.1)** including their cost.

Component	Price per piece (EGP)	Number of pieces	Total price (EGP)
Ferrite plates	100	2	200
Wooden base for coils	150	2	300
Coils	300	2	600
Primary compensating capacitors	15	12	180
Secondary compensating capacitors	10	4	40
High frequency inverter	500	1	500
Miscellaneous	-	-	150
<b>Total</b>			<b>1,970</b>

**Table 9. 1:** Components' Costs

In conclusion a basic static wireless inductive power transfer model would cost around 2,000 (EGP) to construct.

## 9.2. Industrial product

In an industrial model for both static and dynamic wireless power transfer prices would extremely differ, as in industrial products much better and higher quality components are used to achieve the highest possible performance of the system.

For example, a static inductive wireless charger exactly the same as our prototype would cost around five times the cost of the prototype (10,000 EGP) regardless of other expenses which for sure will increase the price of the final product even more.

While for a dynamic system the price would insanely increase, yet increased production lines for the system's products would help in slightly decreasing the system's price. Dynamic wireless power transfer systems were under research for quite a long time now and in the past few years we started to see small systems of kind developed on small scale as the one-kilometer prototype made by Renault at a military base north of France in 2017. Another way was later developed for public use by the public in Norway after the increasing transition to electric cars in Europe, it was said then that such a road costs approximately one million US dollars per kilometer per lane.

But we think through our study and implementation throughout the year such a system could cost around 7.5 million Egyptian pounds (approx. 455,000 USD) that would be the cost per kilometer per lane for the dynamic wireless charging system excluding the cost of implementing the system into the roads and other secondary expenses. The cost estimated excludes any control hypotheses which means it was calculated assuming there is one control inverter for each primary coil, as the price would slightly decrease if each inverter was used for more than one coil through certain control topologies that ensure no overload occurs on any of the inverters.

## 10. Chapter 10: Conclusions

In general, the already presented concepts and demonstration projects related to technology for dynamic inductive power transfer are clearly indicating that this concept is technically feasible. Although a wide variety of concepts have been proposed and investigated at lower power levels, it can also be expected that most of these solutions could be scaled to the power levels and applications that would be needed for transportation of goods.

However, even if it could be theoretically and technically feasible to scale most of the presented concepts to the required power levels, the different concepts have various advantages and disadvantages that would influence their practical applicability. Thus, further research and development efforts are expected to lead towards clearer identification of the most suitable design approaches for various applications.

Furthermore, there are also several remaining research challenges that might influence what will be the most preferable solutions for potential large-scale application of technology for dynamic inductive power transfer. Some of the most relevant issues are listed in the following:

- Coil design.
- Optimal coil section length.
- Optimization of efficiency, performance, and cost.
- Standardization between concepts.
- Interoperability between road-side infrastructure and vehicles with different coil dimensions and different power requirements.
- Control of roadside and vehicle-side conversion stages.
- Cost effective design and construction (ac or dc power distribution systems along the road).
- Integration of the power supply system for the road with the high voltage distribution system.

It should also be mentioned that several theoretical and practical issues associated with the physical construction of the road-side infrastructure would require further attention before large scale application under Nordic conditions. Especially, further investigations and research activities should be conducted towards the integration of coil sections in the road cross-section considering the local requirements for road-construction and the impact of winter conditions and expected mechanical movements in the road structure due to frost.

However, these issues are only indirectly associated with the electromagnetic design of systems for dynamic inductive power transfer. It should be remarked that systems for inductive power transfer in general suffer from higher costs than solutions for conductive power transfer.

The higher costs are mainly due to the need for more active material (i.e. copper, ferrite, capacitors, semiconductors etc.), and the need for additional power electronic converters for generating and controlling the high frequency magnetic field utilized in systems for inductive power transfer. Although ongoing research activities for improvement of the technology for inductive power transfer is not expected to reduce the cost or need of active material to the level of systems for direct conductive power transfer by sliding contacts, the potential advantages of a contactless system can be considered significant.

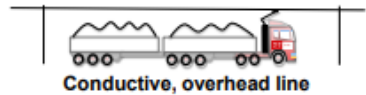
Especially, the advantages in terms of reduced maintenance requirement and simplified system operation that can be expected from a system without any moving parts and where all active components can be encapsulated and protected from mechanical tear and wear can be considered as the main motivations for continued research and development of technology for contactless power transfer.

The technology for dynamic inductive power transfer is currently more diverse than for dynamic conductive power transfer, with several different concepts and design approaches being pursued by different industrial and academic research groups. It should also be expected that the significant ongoing development efforts related to dynamic inductive power transfer will lead to improved performance and increasing power levels in the coming years.

Thus, some of the critical issues for further research and development of the technology has been reviewed. Especially, it is expected that further attention will be dedicated towards standardization and interoperability of various solutions, since this will be necessary for potential future large-scale utilization of such technology.

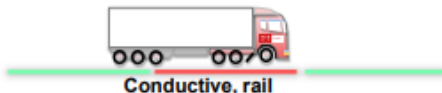
## Different concepts

No in-road installation  
High efficiency



Visual pollution

Multimodal  
High efficiency



Safety  
In-road installation

No visual pollution



Expensive infrastructure  
In-road installation

## Manufacturers milestones:

### BOMBARDIER



**MANHEIM, Germany**  
80m test track  
Research project Slide-in

**Concept:**  
Inductive (10cm, 183kW, 89%, +/- 10cm)

MEASURED

# ALSTOM



## HÄLLERED, Sweden

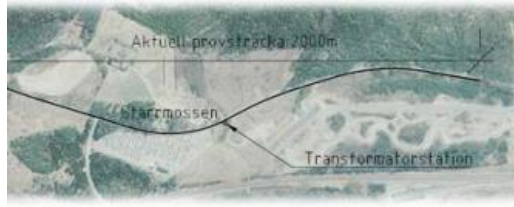
400m test track  
Research project Slide-in

**Concept:**  
Conductive (120kW, 93,3%, +/- 50 cm)

MEASURED



# ELWAYS



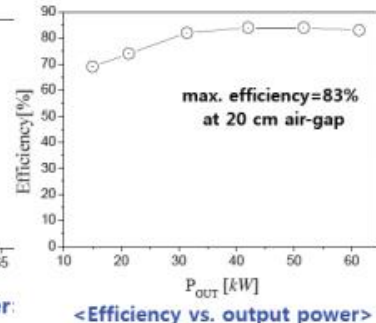
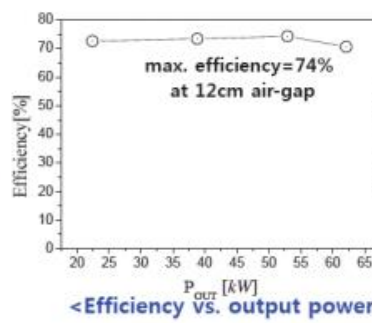
## ARLANDA, Sweden

350m existing test track  
2km public demo (Q3 2017)

**Concept:**  
Conductive



# OLEV TECHNOLOGY



## GUMI, South Korea

Bus in [operation](#) (144m, 2 vehicles)

Research originates from KAIST

### Concept:

Inductive (27cm, 20-200kW,  
74-83%, +/- 20cm)

MEASURED



# Siemens eHighway

Electrified road freight transport – contributing to a sustainable transport sector

**11 %**

of expected truck toll revenue (Lkw-Maut) would cover the investment in a 4,000 km network

**4,000 km**

network of contact lines on German autobahn is recommended by the Federation of German Industries (BDI) as a cost-effective decarbonization measure

**80 %**

of heavy duty trucks would have an economic incentive to switch to contact line, given that the busiest 4,000 km of autobahn are electrified

**16,000 €**

of fuel savings can be achieved by a 40-ton truck driving 100,000 km on the eHighway (based on 1.25 €/l diesel and 0.15 €/kWh electricity)

**>7,000,000 t**

of CO<sub>2</sub> savings per year if 30% of truck traffic on German highways is electrified and supplied with renewables

The key innovation is the active pantograph, capable of connecting while driving at any highway speed

**>80 %**

efficiency level with overhead contact lines

Driving on non-electrified roads (e.g. when overtaking or "first and last mile") is ensured by the hybrid drive technology of the truck and on-board energy storage

Braking energy can be recovered



## Research goals:

**FABRIC**



**Feasibility analysis and development of on-road charging solutions for future electric vehicles**



Italy

### TORINO, Italy

260m test track under development

Testing planned to start Q2 2016

SAET (Inova lab) and POLITO, FIAT

#### Concept:

Inductive (25cm, 20-100kW, 70-80%, +/- 50cm?)

GOALS



France

### SATORY, France

100m test track under development

Qualcomm (Halo IPT), Renault

#### Concept:

Inductive (12,5-17,5cm, 20-40kW, 80%, +/- 20cm)

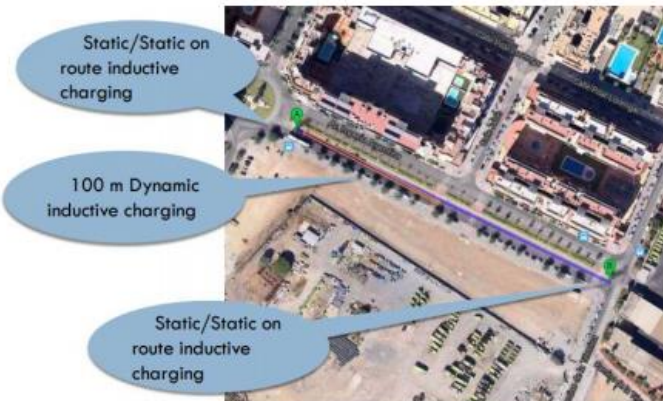
GOALS



## VICTORIA



**Gulliver U520, 5.3 m  
Self-guided control**



### MALAGA, Spain

100 m dynamic with 8 coils (80cm)  
12.5m between each coil  
Test starting in Q1 2016  
Part of "Smart City Malaga" led by Endesa

#### Concept:

Inductive (15-25cm, 50kW, 85%, +/- 30%)

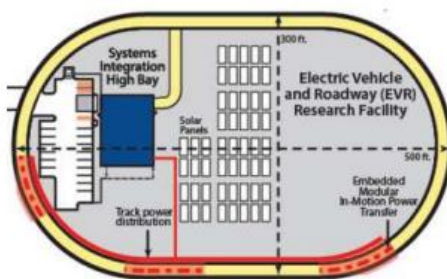
GOALS



## UTAH STATE UNIVERSITY



[WAVE](#) is a spinoff from USU



### LOGAN, UTAH, USA

Demo 20-passenger bus, 2016 Q2  
New research facility (2-3 M\$)

#### Concept:

Inductive (25-35cm, 25-40kW,  
90%, +/- 20cm)

GOALS



## 11. References:

ditya, K., & Williamson, S. (2019). Design Guidelines to Avoid Bifurcation in a Series–Series Compensated Inductive Power Transfer System. *IEEE Transactions On Industrial Electronics*, 66(5), 3973-3982. doi: 10.1109/tie.2018.2851953

Aditya, K. (2017). Analytical design of Archimedean spiral coils used in inductive power transfer for electric vehicles application. *Electrical Engineering*, 100(3), 1819-1826. doi: 10.1007/s00202-017-0663-7

Panchal, C., Stegen, S., & Lu, J. (2018). Review of static and dynamic wireless electric vehicle charging system. *Engineering Science and Technology, An International Journal*, 21(5), 922-937. doi: 10.1016/j.estch.2018.06.015

Covic, G., & Boys, J. (2013). Inductive Power Transfer. *Proceedings of The IEEE*, 101(6), 1276-1289. doi: 10.1109/jproc.2013.2244536

S. M. Lukic, M. Saunders, Z. Pantic, S. Hung and J. Taiber, "Use of inductive power transfer for electric vehicles," in Proc. IEEE PES General Meeting, Minneapolis, MN, 2010, pp 1-6

S. A. Birrell, D. Wilson, C. P. Yang, G. Dhadyalla, and P. Jennings, "How driver behaviour and parking alignment affects inductive charging systems for electric vehicles," *Transportation Research Part C Emerging Technology*, vol. 58, no. PD, pp. 721–731, 2015.

S. Lukic and Z. Pantic, "Cutting the Cord: Static and Dynamic Inductive Wireless Charging of Electric Vehicles," in *IEEE Electrification Magazine*, vol. 1, no. 1, pp. 57-64, Sept. 2013.

Bloomberg - Are you a robot? (2020). Retrieved 16 May 2020, from  
<https://www.bloomberg.com/news/photo-essays/2019-01-05/171-years-before-tesla-the-evolution-of-electric-vehicles>